Published in final edited form as:
Nature. 2021 March 01; 591(7848): 137–141. doi:10.1038/s41586-020-03064-z.

Chromothripsis drives the evolution of gene amplification in cancer

Ofer Shoshani[1], **Simon F. Brunner**[2], **Rona Yaeger**[3], **Peter Ly**[1,4], **Yael Nechemia-Arbely**[1,5], **Dong Hyun Kim**[1], **Rongxin Fang**[1], **Guillaume A. Castillon**[6], **Miao Yu**[1], **Julia S.Z. Li**[1], **Ying Sun**[7], **Mark H. Ellisman**[6,8], **Bing Ren**[1], **Peter J. Campbell**[2,9,10], **Don W. Cleveland**[1,10]

[1]Ludwig Cancer Research and Department of Cellular and Molecular Medicine, University of California at San Diego, La Jolla, CA, USA

[2]Wellcome Sanger Institute, Hinxton CB10 1SA, Cambridgeshire, UK

[3]Department of Medicine, Memorial Sloan Kettering Cancer Center, NY

[4]Present address: Department of Pathology, Department of Cell Biology, University of Texas Southwestern Medical Center, Dallas, TX, USA

[5]Present address: Hillman Cancer Center, Department of Pharmacology and Chemical Biology, University of Pittsburgh, Pittsburgh, PA, USA

[6]National Center for Microscopy and Imaging Research (NCMIR), University of California San Diego, La Jolla, CA, USA

[7]Department of Pediatrics, University of California at San Diego, La Jolla, CA, USA

[8]Departments of Neurosciences and Bioengineering, University of California San Diego, La Jolla, CA, USA

[9]Department of Haematology, University of Cambridge, Cambridge CB2 2XY, UK

Abstract

Focal chromosomal amplification is an important route to generating cancer through mediating over-expression of oncogenes[1–3] or to developing cancer therapy resistance by increasing expression of a gene whose action diminishes efficacy of an anti-cancer drug. Here we used whole-genome sequencing of clonal isolates developing chemotherapeutic resistance to identify

[10]**Corresponding authors:** Correspondence to Don W. Cleveland (dcleveland@ucsd.edu) and Peter J. Campbell. (pc8@sanger.ac.uk).

Author contributions

O.S. and D.W.C. conceived the project and wrote the manuscript. O.S. designed, performed, and analyzed all experiments not otherwise specified next. O.S. and P.L. performed HSR evolution experiments. O.S. and Y.N-A. tested drug treatment concentrations, O.S. and D.H.K. performed live cell imaging and performed DM integration experiments following Cas9 expression, R.Y. obtained human DNA samples and FISH of human biopsies. O.S. and J.L. designed sgRNA for Cas9 experiments. S.F.B., P.J.C., and O.S. performed and analyzed the DNA sequencing experiments. O.S., S.F.B., and Y.S. analyzed the RNA sequencing data. O.S. and M.Y. performed the HiC experiments. O.S., R.F., and B.R. analyzed the HiC sequencing data. G.H.C. and O.S. performed the CLEM experiments. O.S., G.H.C., and M.H.E. analyzed the CLEM experiments. All authors provided input on the manuscript and D.W.C., P.J.C., and O.S. supervised all aspects of the work.

Competing interests

The authors declare no competing interests.

Europe PMC Funders Author Manuscripts

chromothripsis as a major driver of extrachromosomal DNA (ecDNA) amplification into circular double minutes (DMs) through PARP- and DNA-PKcs-dependent mechanisms. Longitudinal analyses revealed that DMs undergo continuing structural evolution to promote increased drug tolerance through additional chromothriptic events. *In-situ* Hi-C sequencing is used to demonstrate that DMs preferentially tether near chromosome ends where they re-integrate when DNA damage is present. Intrachromosomal amplifications formed initially under low-level drug selection undergo continuing breakage-fusion-bridge cycles, generating >100 megabase-long amplicons that we show become trapped within interphase bridges and then shattered, producing micronuclei that mediate DM formation. Similar genome rearrangement profiles linked to localized gene amplification are identified in human cancers with acquired drug resistance or with oncogene amplifications. We propose that chromothripsis is a primary mechanism accelerating genomic DNA amplification and which enables rapid acquisition of tolerance to altered growth conditions.

Gene amplification was first identified[4] in cells developing resistance to methotrexate, an inhibitor of dihydrofolate reductase (DHFR) that has been used for over 50 years as an anticancer therapeutic. Amplified DNA can be found in small circularized DNAs referred to as double minutes (DMs)[5], a sub-type of extra-chromosomal DNA (ecDNA)[2], or in intra-chromosomal homogenously staining regions (HSRs)[6]. Previous studies suggested that DMs can integrate into host chromosomes[7,8] and that HSRs could be a potential source of DMs[2,9,10]. Use of whole genome sequencing has provided high resolution views of genome rearrangements across human cancers[11–13], including gene amplification and chromothripsis[14–16], the catastrophic shattering of a chromosome followed by fragment religation in random order. Different mechanisms have been proposed to drive DM formation, including chromosome breakage leading to simple circularization of an excised chromosome segment or co-ligation of multiple fragments induced by chromothripsis[14,17–21]. HSR formation can also be an outcome of multiple mechanisms: breakage-fusion-bridge (BFB) events, as identified by McClintock in the 1940s[22], intra-chromosomal tandem duplications[23], or neochromosomes seen in sarcomas[24]. Here we examine the interplay between intra- and extra-chromosomal amplifications, and the evolution of these structures in response to increased selection pressure.

Chromothripsis drives ecDNA amplification

To determine the mechanisms underlying early acquisition of drug resistance and subsequent dynamics, we applied tunable selection pressure using different concentrations of methotrexate (Fig. 1a). Although the initial HeLa karyotype is abnormal, it was found to be stable (Extended Data Fig. 1a), with chromosome 5 content in all primary clones (and the parental HeLa population) consistent with previous reports[20,25]. Clones were subjected to a one-step methotrexate treatment using one of three concentrations (based on testing of effective dose responses – Extended Data Fig. 1b) and 57 resistant colonies were collected, of which 28 were determined by DNA fluorescence *in situ* hybridization (FISH) to have amplified *DHFR* within DMs or HSRs (Fig. 1a). Application of weak, continuous selection pressure typically generated simple, low-level copy number gains, whereas continuous, stronger selection pressure promoted DM formation (Figure 1a). Both types of

amplifications occurred early, as in initial resistant colonies (100-200 cells) the HSRs or DMs were found in all cells (Extended Data Fig. 1c).

Paired-end whole genome sequencing (WGS) was used to determine the genomic rearrangements of five control and 18 resistant clones (Fig. 1b). WGS data perfectly coincided with karyotyping by DNA-FISH and RNA expression measured with RNA sequencing (Extended Data Fig. 1d). *DHFR* DNA copy number and RNA level were highly correlated (R^2=0.85, Extended Data Fig. 1e). Resistant clones without *DHFR* amplification showed no increase in *DHFR* expression but had a distinct gene expression profile (1,438 differentially expressed genes) (Extended Data Fig. 1f).

While (as expected) control clones had acquired no new genome rearrangements, three different profiles consistent with chromothripsis as the trigger of ecDNA formation and amplification as DMs were identified in resistant clones (Fig. 1c-e). In the first, a chromothriptic rearrangement of one chromosome 5 excised a single fragment containing the *DHFR* gene which then circularized into a DM (Fig. 1c and Extended Data Fig. 2a-c). In the second profile, multiple (4-17) chromothriptically produced, non-contiguous fragments from chromosome 5 (as far as 80 Mb apart on the initial chromosome and including *DHFR)* were circularized and amplified (Fig. 1d and Extended Data Fig. 2d-k). In the third profile, an entire copy of chromosome 5 was lost except for a DM circularized from a single fragment containing *DHFR* (Figure 1e and Extended Data Fig. 2m-n) which appeared subsequently to have undergone additional rearrangements[26].

These profiles are representative of rearrangements arising from selection, as two additional cell lines (HT-29 colon cancer cells and 293T human embryonic kidney cells) treated with methotrexate generated similar *DHFR* amplification through chromothripsis (Fig. 1f-g and Extended Data Fig. 2o-p). Breakpoint junction analysis of the eight chromothriptic DM positive HeLa clones (summarized in Extended Data Fig. 2q) revealed non-templated insertions with minimal microhomology sequences (Fig. 1h). Non-homologous end joining (NHEJ) was needed for efficient DM formation, as inhibition of it (with DNA-PKcs or poly-ADP-ribose polymerase (PARP) inhibitors added at concentrations with minimal effect on viability - Extended Data Fig. 2r) significantly decreased frequency of both resistant colony formation (Fig. 1i) and DM production (Fig. 1j).

Finally, to test the generality of chromothripsis in drug-mediated gene amplifications, pre- and post-treatment biopsies from colorectal cancers or their metastases were analyzed from two individuals whose cancers were caused by the kinase activating mutation V600E in BRAF and who developed resistance to therapy with vemurafenib, a selective inhibitor of this BRAF mutation[27]. Vemurafenib resistance in one patient was accompanied by copy number jumps of $BRAF^{V600E}$ and inversions typical of BFB (Fig. 1k, Extended Data Fig. 3a-b, and Supplementary Table 1). A second patient developed amplification of the $BRAF^{V600E}$ gene through chromothripsis, with a BRAF gene-containing fragment ligated together with a second fragment initially 10 Mb upstream into a DM containing multiple additional rearrangements, consistent with one or more subsequent rounds of chromothripsis (Fig. 1l, Extended Data Fig. 3c-d, and Supplementary Table 1).

Chromothripsis drives DM evolution

Next, we examined DM evolution during adaptation to an increased methotrexate concentration (Extended Data Fig. 4a). Stepwise drug increase led to elevated DM copy number (Fig. 2a and Extended Data Fig. 4b) and major structural changes resulting in up to a 10-fold increase in *DHFR* gene copies per DM, as determined by intensity of the FISH signal (Fig. 2b and Extended Data Fig. 4c). WGS revealed that two clones contained DMs with a common rearrangement profile at basal drug concentration (Extended Data Fig. 4d). An initial “simple” 2.1 Mb DM in clone PD29429h (Fig. 2c) underwent chromothriptic rearrangement during adaptation to increased methotrexate, forming one or more DMs (see variation in read coverage – Extended Data Fig. 4e) with more complex rearrangements (Fig. 2d) that were undetectable prior to methotrexate increase (Extended Data Fig. 4f), consistent with multiple co-evolving DMs produced by subsequent round(s) of chromothripsis acting on one or more copies of the initial DM.

Indeed, *DHFR*+ micronuclei were present in almost two thirds (65%) of cells resistant to the higher concentration of methotrexate (Fig. 2e, Extended Data Fig. 4g), indicative of ongoing production of substrates for additional chromothriptic events[26,28]. Similar structural instability was also observed in a second HeLa DM clone (Extended Data Fig. 4d) and in HT-29 cells (Fig. 2f-i) subjected to increased methotrexate concentration. *In silico* simulations of DM selection were performed assuming DMs assorted randomly to daughter cells (as determined in Extended Data Fig. 4h) from a cell with an initially defined set of DMs, only one of which carried multiple copies of the resistance gene. These analyses confirmed the advantage conferred by DMs with more than one copy of the resistance gene independent of initial DM number (Extended Data Fig. 4i-l). Thus, escalating selection pressure drives structural evolution of an initial DM through repeated rounds of chromothripsis, yielding DMs containing increased number of copies of the target gene per DM.

DNA damage drives ecDNA integration

Previous studies showed that ecDNA elements can integrate into chromosomes[2,7,8]. We initially tested the role of DNA damage in this process by inducing random double-strand breaks in clonal DM-positive cells using ionizing radiation or doxorubicin (Extended Data Fig. 5a-b) or by inducing specific double-strand breaks using nucleases targeting a site 3.5 Kb from *DHFR* found on chromosome 5 as well as on the DMs (Extended Data Fig. 5c). DM integrations forming ectopic HSRs (eHSRs) were identified in up to 30% of scored spreads following either random or specific double-strand break induction (Extended Data Fig. 5a-c). To directly test if DMs integrate into sites of DNA damage, we induced double-strand breaks at three different locations on chromosome 3 using Cas9 and identified DM integrations at these specific ectopic DNA sites in up to 17% of cells (Figure 3a).

In most (70%) cases following random DNA damage, DM integration occurred at an ectopic site near a chromosome end (Extended Data Fig. 5a-c). Treatment with a PARP inhibitor, but not with an inhibitor of DNA-PKcs, resulted in 3-fold increased frequency of such eHSRs, most of which (78%) inserted within 10 Mb of a chromosome end (Extended Data Fig. 5d).

PARP inhibition also significantly increased the frequency of DM conversion into eHSRs in Colo320DM-GFP cells[29] (Extended Data Fig. 4e) and of enlarged DMs (Extended Data Fig. 4f-g). Consistent with previous work suggesting integrations occur near telomeres[7,8], use of unbiased, genome-wide *in-situ* Hi-C sequencing identified significant linkage of DMs with chromosome ends in both mitotically-arrested cells and cycling cells (Extended Data Fig. 5h-j).

To determine eHSR structures, 25 subclones resistant to increased methotrexate in the presence of a PARP inhibitor were isolated from an initial DM-containing clone. Four (16%) contained clonal events of DM integration producing an eHSR in all cells, three of which were located near a chromosome end (Fig. 3b-e). The eHSRs of all four clones showed distinct rearrangement profiles derived from the parental DM population (see also breakpoint PCR – Extended Data Fig. 4e). One clone carried a large (40 Mb) eHSR initially integrated 60 Mb from a telomere of chromosome X (Fig. 3d), producing a region susceptible to breakage and formation of dicentric chromosomes that drive BFB cycles (Fig. 3d). Finally, two eHSRs shared the same amplified region (Fig. 3b,d) with one presenting massive rearrangements with multiple proximal (Kb scale) integration sites within 1.1 Mb of the tip of chromosome 3, suggesting either multiple DM integrations or a single integration of a massively rearranged DM containing multiple *DHFR* copies (Fig. 3b).

BFB with subsequent chromothripsis

The evolution of HSRs was examined in response to stepwise elevation in selection pressure. A small HSR initially generated by two cycles of BFB following methotrexate treatment was identified to carry four *DHFR* copies (Extended Data Fig. 6a-h). Adaptation to elevated drug concentration resulted in DM acquisition that was coupled with loss of the HSR (Extended Data Fig. 6i). WGS of one clone revealed a complex, 1.4 Mb DM with 14 non-adjacent regions of the HSR derived by chromothriptic shattering and re-stitching in random order and with variable copy numbers of individual pieces (Extended Data Fig. 6j). Evidence of BFB followed by chromothripsis was found in other resistant clones. Clone PD29427p presented an HSR that underwent complex rearrangements consistent with localized chromothripsis of chromatin trapped in an interphase DNA bridge (Extended Data Fig. 7a-c). Two DM containing clones (Fig. 1c and Extended Data Fig. 2b) which maintained the chromothriptic chromosome of origin showed features of BFB-chromothripsis (including complete loss of the 5q region telomeric to *DHFR* and increased copy number of some fragments). Kataegis, a hypermutation signature recently associated with chromothripsis of dicentric chromosomes[30], was detected in nearly half (3 of 8) of DM clones, consistent with evolution from an initial HSR (Extended Data Fig. 7d-e).

Evolution of an HSR into DMs was followed during adaptation to a higher methotrexate dose (Fig. 4a; Extended Data Fig. 8a-c). Over two weeks, HSR size tripled (Extended Data Fig. 8d-e), with a sharp (55%) increase by day 10 in the frequency of dicentric HSRs (Extended Data Fig. 8f-g). Live-cell imaging revealed that at 10 days 40% of mitoses had anaphase bridges which frequently persisted into interphase (Extended Data Fig. 8h and Supplementary Video 1). In the next division, daughter cells either formed another bridge (40%), consistent with ongoing BFB (Extended Data Fig. 8i and Supplementary Video 1), or

the dicentric state was resolved possibly through chromothripsis or telomere capture (60%). Strikingly, by day 12 almost 30% of cells had *DHFR*+ HSRs trapped within interphase bridges (Fig. 4b-c). Rupture of interphase bridges observed by live-cell imaging resulted in the formation of *DHFR* gene-containing nuclear bulges (Extended Data Fig. 8j) and production of *DHFR*+ micronuclei (Fig. 4d and Extended Data Fig. 8k).

WGS of one HSR+ clone and a derivative DM+ population resulting from two-week exposure to increased methotrexate revealed that during selection the initial HSR (produced through five BFB cycles) was shattered (along with adjacent regions of chromosome 5) to produce highly rearranged DMs (Fig. 4e-f). BFB with chromothripsis was also observed in methotrexate resistant 293T cells initially containing a *DHFR*+ HSR that converted into DMs with increased drug concentration (Extended Data Fig. 8l-m). In HeLa cells resistant to mitotic kinesin inhibitor S-trityl-L-cysteine (STLC), chromothripsis promoted the resolution of BFB-induced *Kif15* amplification by capturing a telomere from chromosome 1 (Extended Data Fig. 9). Finally, formation of DMs through BFB-chromothripsis was highly dependent on NHEJ, as DM formation was significantly inhibited by addition of a DNA-PKcs inhibitor (Fig. 4g).

Examination of interphase DNA bridges in HSR+ cells adapting to increased methotrexate or in cells adapting to the DNA damaging agent zeocin identified many instances of micronuclei formed within the bridge (Fig. 4h, Extended Data Fig. 10a-c, and Supplementary Video 2), consistent with a prior report that micronuclei can form following anaphase bridge resolution[31]. Ingression of the cleavage furrow disrupted nuclear envelop structure of a nucleus/micronucleus caught between nascent daughter cells (Extended Data Figure 10d). DNA in bridges juxtaposed to the midbody had aberrant nuclear envelopes and appeared compartmentalized (Extended Data Fig. 10e). DNA and midbody signals were mutually exclusive, consistent with the midbody as a site of DNA cleavage (Extended Data Fig. 10f). Micronuclei formed after bridge resolution had highly abnormal nuclear envelopes (Extended Data Fig. 10g), serving as a chromothriptic source[26] to DM formation (Fig. 4i).

Chromothriptic oncogene amplifications

We next examined if the chromothriptic origin of gene amplification seen in response to DHFR, $BRAF^{V600E}$, and kinesin inhibitors was representative of additional human cancers. Comparison of the genomic profiles of HeLa cells with *DHFR* amplification and glioblastoma multiforme (GBM), a cancer with a high frequency of DMs[2], revealed that both shared a similar random distribution of rearrangements (Extended Data Fig. 11a,b). Further, a comparison of copy number profiles of the amplified *DHFR* locus to a panel of 15 different cancers containing oncogene amplifications (Extended Data Fig. 11c-d) revealed similar localized amplifications in randomly rearranged chromosomes (Extended Data Fig. 11d-e). Finally, breakpoint junction analysis revealed non-homologous end-joining as the dominant form of repair (Extended Data Fig. 11f) leading to amplifications.

Chromothripsis and cancer therapy

We have identified mechanisms accessed by cancer cells in which chromothripsis drives the evolution of amplified DNA (Extended Data Fig. 11g). Our findings bridge two biological phenomena discovered more than 70 years apart: cycles of break-fusion-bridge[22] (with subsequent HSR formation) and chromothripsis[14] of either micronucleated DNAs[26,28] or interphase chromosome bridges (Fig. 4 and ref.[30]). Our work identifies NHEJ and PARP-dependent repair after chromothriptic shattering both as a mechanism generating initial oncogene amplification or anti-cancer drug resistance and as a driver of subsequent rearrangements. Recognizing that chemotherapeutic drugs (e.g., methotrexate or vemurafenib) can lead to chromothriptically initiated rearrangements, combination of a targeted therapy with DNA repair inhibitors[32] may represent an effective approach to prevent an initial cancer from becoming more aggressive or drug resistant.

Methods

Cell culture

HeLa S3 (authenticated using WGS and FISH) and 293T (authenticated by frequent use for transfection and lentiviral particle preparation, and by morphology and growth in culture) (both lines are from the Cleveland lab cell stock), and DLD-1 (fresh from ATCC) cells were grown in DMEM (Gibco) containing 10% fetal bovine serum (Omega), supplemented with 100U/ml penicillin, 100U/ml streptomycin, and 2mM l-glutamine, at 37°C in a 5% CO2 incubator. When treating with methotrexate, dialyzed fetal bovine serum was used instead (Gibco, 26400044). HT-29 cells were obtained fresh from ATCC and grown in McCoy's 5A (Gibco) containing 10% fetal bovine serum (Omega), supplemented with 100U/ml penicillin, 100U/ml streptomycin, and 2mM l-glutamine, at 37°C in a 5% CO2 incubator. T-47D were obtained fresh from ATCC and grown in RPMI-1640 with supplements as above. Colo320DM-GFP (authenticated by having GFP+ labeled DMs, and by morphology in culture), a kind gift of Noriaki Shimizu (Hiroshima University, Japan), were grown in RPMI (Gibco) containing 10% fetal bovine serum (Omega), supplemented with 100U/ml penicillin, 100U/ml streptomycin, and 2mM l-glutamine, at 37°C in a 5% CO2 incubator. Cells were periodically tested for mycoplasma and confirmed free of contamination. Cell lines used in this study are not found in the list of commonly misidentified cell lines maintained by the International Cell Line Authentication Committee.

Isolation of methotrexate resistant clones

HeLa S3 cells were subjected to two rounds of single cell cloning. In the first round, five primary clones were isolate from a 96-well plate in which 0.5 cells/well were seeded. Subsequently, each of the five primary clones was seeded at 0.5 cells/well in 96-well plates to isolate six secondary clones from each of the primary clones (a total of 30 secondary clones were collected). All clones collected were verified microscopically to be single cell derived. HeLa clones were then subjected to treatment with either 40nM, 60nM, or 80nM methotrexate for a duration of up to one month, with media replaced twice per week. Individual surviving colonies were picked and transferred to a 24-well plate and later to a 6-well plate, from which cells were collected for FISH, RNA, DNA, and storage.

Colony forming assay

Cells were seeded at low dilution and colonies formed (number of cells seeded, and time of culture are indicated in each experiment) were methanol fixed and stained with a 0.5% crystal violet, 20% ethanol solution. Plates were photographed using Gel Doc XR+ (Bio-Rad) and colonies were manually quantified.

Reagents

DNA damage repair inhibitors were dissolved in DMSO and used at the following concentrations: 15 μM ABT-888 (PARP inhibitor, Enzo), 10 μM Olaparib (PARP inhibitor, ApexBio), and 10 μM NU7026 (DNA-PKcs inhibitor, Abcam). Methotrexate (454126, Calbiochem) was dissolved in DMSO and used at indicated concentrations. Doxorubicin (Sigma) was dissolved in water and cells were treated at a final concentration of 0.5 μM for 1 hour. Hydroxyurea (Sigma) was dissolved in PBS and used at a final concentration of 100 μM. S-Trityl-L-cysteine (STLC, Sigma) was used at a final concentration of 10μM, and zeocin (Gibco) was used at a final concentration of 100μg/ml.

Site specific nucleases

For Figure 3a: Dox-inducible lentiviral expression of SpCas9 construct, pCW-Cas9 was obtained from Addgene (50661). Lentiviral sgRNA expressing construct were made by inserting guide sequences into two BbsI sites of pLH-sgRNA1 from Addgene (75388). To generate lentiviruses, 293T cell were transfected with sgRNA-concstruct, psPAX2 and pMD2.G plasmids. Guide sequences were designed using the Broad Institute portal (https://portals.broadinstitute.org/gpp/public/analysis-tools/sgrna-designhttps://portals.broadinstitute.org/gpp/public/analysis-tools/sgrna-design). gRNA#1: GAAGCCACCATGTCTCACCA; gRNA #2: CTGAAAGTCCTCGGTCTGAC; gRNA #3: TGATATCACAG; gRNA #4: GCTGAAGAGATTTACAGTCC.

For Extended Data Figure 5c: Transcription activator-like effector nuclease (TALEN) targeting a location approximately 3500bp centromeric to the *DHFR* locus (80622611 Mb – 80622657 Mb on chromosome 5) and containing the sequence: t**ctgctgaagagattt**acagtcctggtcccc**attttctcttattct**a (TALEN recognition sites in bold) was assembled using the golden gate reaction as previously described[33]. CRISPR/Cas9 targeting the site 5’ GCTGAAGAGATTTACAGTCC 3’, near the same location as TALENs (80622635 Mb – 80622654 Mb) was constructed by inserting the sgRNA sequence into a wild-type Cas9 vector (Addgene 42230) as described before[34]. HeLa cells were transfected with either the TALEN or CRISPR/Cas9 expression vectors by nucleofection (Lonza) using solution R and program I-013 and efficient cutting was validated using specific primers and the surveyor assay kit (Transgenomics) as previously described[34].

DNA fluorescent in-situ hybridization (FISH)

Chromosome spreads were obtained by dropping mitotic cells on glass slides. In short, cells were arrested for 3 hours with 100 ng/ml colcemid (KaryoMAX, Thermo Fisher), and then incubated in 75mM KCl for 15 minutes at 37 °C. Cells were fixed by adding methanol/acetic acid (3:1), washed with fixative three times, and kept in fixative at -20 °C until use. For

interphase FISH, cells growing on poly-l-lysine coated coverslips (Corning) were washed with PBS and fixed using methanol/acetic acid (3:1) and kept in fixative at -20 °C until use. To make custom BAC probes, the following BACs were ordered from bacpac (https://bacpacresources.org/): RP11-90A9 (*DHFR*, used throughout the manuscript), RP11-538B23 (DHFR, used to validate first BAC), RP11-440N18 (*MYC*), for chromosome 5 rearrangements analysis: RP11-958F12, RP11-314L7, RP11-33C19, and for Kif15 amplification analysis: RP11-659N22 and RP11-372G3. BACs were isolated from 50ml bacterial cultures using the BACMAX Bac extraction kit (Epicentre). Isolated BACs were sonicated (x10 cycles of 15 seconds 'on' 45 seconds 'off' at constant intensity with power set to '3', Branson sonifier 450) and labeled with either TM-rhodamine or cy5 using Label-IT (Mirus). Labeled BAC probes were suspended in commercial chromosome paint probes (Metasystems). DNA-FISH was performed by applying probes onto samples and covering with a glass coverslip. Genomic DNA and probes were co-denatured at 75 °C for 2 minutes by placing slide on pre-heated metal plate. Samples were hybridized overnight at 37 °C in a dark humidified chamber. Slides were subsequently washed with 0.4× SSC at 72 °C for 2 min and rinsed in 2× SSC, 0.05% Tween-20 at room temperature for 30 s. Slides were then rinsed in PBS, counterstained with DAPI, and mounted using pro-long gold (Invitrogen). FISH images were acquired on a DeltaVision elite system (Applied Precision) at either ×60 or x100 magnification (10 × 0.5 μm z-sections). Deconvolution and maximum intensity projections were generated using the softWoRx program.

Measurements of gene amplification

DM and micronuclei numbers were manually counted. DM intensities relative to the endogenous DHFR on chromosome 5 were determined using the ROI feature in Fiji (ImageJ)[35] by averaging the intensities of the brightest four single DM dots in each spread and subtraction of similarly sized adjacent background regions, divided by the average intensity of the endogenous DHFR signals within the same spread (with background subtracted). HSR lengths were measured (Fiji) and normalized to the normal chromosome 5 length within the same spread for comparison.

Live cell imaging

To study the events occurring in HSR positive cells after increasing methotrexate concentration, one million HSR+ clone 28e (resistant to 60nM methotrexate) were treated with 500nM methotrexate for 10 days in a 10cm culture dish from which 5,000 cells per well were seeded in a polystyrene glass 96-well plate. One day later, cells were stained with DNA SiR (1:2000 from a stock of 50nmol in 50 μl DMSO, Cytoskeleton, CY-SC007) and verapamil (1:2000 from a stock of 1 μmol in 100 μl DMSO, Cytoskeleton, CY-SCV01), and 2 hours later were imaged using a CQ1 spinning disk confocal systems (Yokogawa Electric Corporation) with a x40 magnification at 37°C and 5% CO2. Image acquisition and data analysis were performed using CQ1 software and ImageJ, respectively. Images of 20 fields/well at 8 × 3-μm z-sections in cy5 were acquired at 10 minutes intervals for 48 hours. The mitotic fate of parental and daughter cells (two cell cycles) was analyzed and scored for formation of micronuclei and/or DNA bridges. Proliferation rate was automatically determined using the CQ1 software by automated counting of the number of cells per field per each time point, and data was plotted using Prism GraphPad.

Immunofluorescence

Cells were plated onto poly-L-lysine coated coverslips (Corning) and fixed in 4% formaldehyde for 10 mins at room temperature. Cells were incubated in blocking solution (0.2 M Glycine, 2.5% FBS, 0.1% Triton X-100, PBS). The following primary antibodies were used at 1:200 dilution in blocking solution and washed with 0.05% Tween in PBS: Aurora B (Abcam, ab2254), Lamin B (Proteintech, 12987-1-AP). Actin was labeled using Alexa Fluor 647 phalloidin (Thermo Fisher Scientific). Images were acquired on a DeltaVision elite system at 40–60× magnification (8 × 0.5 μm z-sections) and deconvolved maximum intensity projections were generated using softWoRx program.

Cell cycle analysis

Ethanol-fixed cells were stained with 10 μg/ml propidium iodide and 50 μg/ml RNase A and analyzed for DNA content by flow cytometry on a BD LSR II instrument (BD Biosciences) using BD Cellquest software.

ChromEM: DRAQ5 DNA labeling, DAB photo-oxidation, and osmium tetroxide staining

For ChromEM, the samples were treated as in[36]. Cells were shortly washed in PBS without calcium and magnesium, then fixed with 2.5% EM grade glutaraldehyde (Electron Microscopy Sciences) in 5 mM CaCl2, 0.1 M sodium cacodylate buffer, pH 7.4, at room temperature for 2 minutes and for an additional hour on ice. From this step on, the cells were always treated either on ice or on a cold stage set at 4˚C. All solutions were at 4˚C before applying to cells. Fixed cells were washed 3 times for two minutes in 0.1 M sodium cacodylate buffer. Cells were blocked for 15 minutes using blocking buffer (10 mM glycine, 10 mM potassium cyanide in 0.1 M sodium cacodylate buffer). DNA was stained with DRAQ5 (5 μM) in 0.1 M cacodylate buffer for 30 minutes followed by 3 x 5 minutes washes with blocking buffer. After washing away excess dye, cells were bathed in 2.5 mM diaminobenzidine tetrahydrochloride (Sigma) in 0.1 M sodium cacodylate buffer. Cells were placed on a Leica SPE-II confocal microscope with a custom cold stage set at 4˚C and imaged using a 63x oil immersion objective lens (NA = 1.3) and Cy5 filter set (620 ± 30 nm). After 3D imaging in the DIC channel and the DRAQ5 fluorescence, cells were photo-oxidized by continuous epi-fluorescence illumination (150W Xenon Lamp) for 2 minutes. DIC was taken one more time to verify the reaction of photo-oxidation. Cells were rinsed 5 x 2 minutes with 0.1 M sodium cacodylate buffer. Cells were stained for 30 minutes with 2% osmium tetroxide, 2 mM CaCl2, 1.5% potassium ferrocyanide in 0.15 M sodium cacodylate buffer. Cells were washed with double distilled water 5 x 2 minutes. Cells were additionally incubated for 2 hours in 2% uranyl acetate in double distilled water and washed with double distilled water 5 x 2 minutes before dehydration.

EM sample preparation and TEM

Cells were dehydrated in ethanol and embedded in Durcupan epoxy resin as described previously[37]. Epoxy embedded cells were cut into 70nm sections and mounted on 200 hexagonal mesh copper grids. Sections were post stained 3 minutes in 2% uranyl acetate in double distilled water followed by 4 washes in double distilled water, then incubated for 2minutes in Sato Lead, and finally washed 4 times in double distilled water. Sections were

imaged at 120keV with a FEI/Thermofisher Tecnai G2 Spirit. Images and montages were acquired with serial EM and stitched with Etomo.

Breakpoint PCR

Primers specific for breakpoints (junctions of non-contiguous fragments) found were designed using whole-genome sequencing data. Primers for breakpoints found in clone 1 640nM and eHSR clone 29s: 5' ACCACAATTCAGCTAACTCCACT 3' and 5' TTTGAAGAGTCCTTGCCATTGTC 3'. Primers for breakpoints found only in clone 1 640nM: 5' CCTCGTGTTATTCTTTGGCCTG 3' and 5' TTGAAAGCGAACGTCACTGAG 3'. Primers for breakpoints found in clone 1 160nM and 640nM and eHSR clone 29s: 5' CCCCACATAACCCTGAGCTG 3' and 5' TGGTAGGAGCAACCTGCTTT 3'. Full scans of gels are provided in Supplementary Information.

In situ Hi-C sequencing

In-situ Hi-C experiments were performed as previously described[38]. Cells were fixed with 1% of formaldehyde at room temperature for 10 minutes. After inactivating with glycine, crosslinked cell pellets were washed with cold PBS once before snap freezing with liquid nitrogen. 1-3 million crosslinked cells were used per Hi-C experiment as follows: Briefly, the crosslinked cell pellets were thawed on ice, lysed on ice for 15 minutes (lysis buffer: 10 mM Tris, pH 8.0, 10 mM NaCl, 0.2% IGEPAL CA-630 with proteinase inhibitor) followed by a washing with lysis buffer. The pellets were then resuspended in 50 μl 0.5% of SDS and incubated at 62°C for 10 minutes. Permeabilization was quenched by adding 25 μl 10% Triton X-100 and 145 μl water, and incubation at 37°C for 15 minutes. Digestion was performed overnight at 37°C, shaking at 1,000 rpm with 1xNEBuffer 2 and 100 units of MboI, followed by inactivation of MboI at 62°C for 20 minutes. Biotin fill-in reaction was performed for 1.5 hours at 37°C with 15 nmol of dCTP, dGTP, dTTP, biotin-14-dATP each and 40 unit of Klenow. In-situ ligation was then performed at room temperature with slow rotation in a total volume of 1.2 ml containing 1xT4 ligase buffer, 0.1mg/ml BSA, 1% Triton X-100 and 4000 unit of T4 ligase. After ligation, the DNA was reverse crosslinked at 55°C for 30 minutes followed by 68°C overnight in the presence of SDS, NaCl and proteinase K. Afterwards, DNA was extracted by ethanol precipitation and then sheared to an average of 400bp with Covaris M220. Ampure beads were used to further purify the sheared DNA and select the fragments between 300 to 700bp. The biotin pull-down enrichment and library construction were performed as previously described[38] and sequenced using HiSeq 4000 (Illumina). Hi-C data processing was performed as follows: Paired-end HiC sequencing reads were mapped using BWA-MEM to the reference genome (hg19) in single-end mode with default parameter setting for each of the two ends separately. The independently mapped ends were then paired-up and the read pairs were kept if both ends uniquely mapped to the genome (MQAL>10). Next, read pairs were further removed if either end was mapped more than 500bp apart away from the closest MboI cutter site. Read pairs were next sorted based on genomic coordinates followed by PCR duplicate removal using samtools rmdup. Processed Hi-C data is converted to .hic file and is visualized using juicebox without normalization. The following analysis was performed to quantify the interaction frequency between DM sequences and the rest of the genome: (1) Each Hi-C read pair contains two reads that are mapped to two different loci on the genome indicating one captured

interaction between these two loci. We first extracted all Hi-C read pairs (called DM pairs) that has one read mapped within the DM region and the other end is aligned outside DM region (excluding chr5). (2) We then segmented the genome into a set of bins of equal length (1Mb). (3) Next, using the DM pairs obtained from step 1, for each 1Mb bin obtained from step 2, we counted the number of reads falling into each bin. (4) Finally, for every sample, the interacting frequency is normalized to RPM (reads per million reads) by the total number of DM pairs. (5) To compare two samples, we normalized the interacting frequency of one sample with the interacting frequency of another sample (control sample).

RNA sequencing

Global gene expression profiling was done on total RNA extracted using the Nucleospin RNA kit (Macherey-Nagel) and processed using the Illumina TruSeq Stranded mRNA Sample Preparation Kit. Then, cDNA libraries were sequenced on an Illumina HiSeq 4000 using single read, 50 cycle runs. Quality of sequencing reads was assessed using FastQC (Babraham Bioinformatics) and aligned to a reference genome (hg19, UCSC Genome Browser) using TopHat. Sequencing yielded on average 46.3 million reads per sample with a ~71% mapping rate to generate ~33 million reads per sample uniquely mapped to the reference genome. Cufflinks was used to generate transcript abundance as fragments per kilobase of transcript per million mapped reads (FPKM), and statistical analysis of FPKM values was calculated using R (Bioconductor). RNA expression (relative to control) was plotted on a linear map of chromosome 5. Genes which expressed [FPKM>=1] were kept for downstream Principle Component Analysis (PCA). And semi-unsupervised (gene unsupervised and sample supervised) hierarchical clustering with complete method was applied on the heatmap.

Colorectal cancer patient analysis

Patient data was previously reported in Yaeger, R. et al 2017[27]. Collection and analysis of patient samples was conducted under appropriate Institutional Review Board/Privacy Board protocols and waivers (MSKCC protocols 19-323, 06-107). Participating patients provided signed written informed consent. The study was conducted in accordance with the ethical guidelines in the Declaration of Helsinki.. Patient DNA was sequenced at the Sanger Institute using Whole Genome Paired-end sequencing at a coverage of x60-x130. Pre-treatment biopsies showed no evidence of BRAF amplification. Progression samples were assigned a sample number with no patient identifying information before submission for DNA extraction and genomic analysis. No one performing genomic analysis had access to the patients' identifying information.

X-ten sequencing

DNA from the pre- and post- methotrexate exposed samples was extracted using the DNeasy kit (Qiagen, 69504) according to manufacturer guidelines and was sequenced on the Illumina X10 platform to a target coverage of 30x whole human genome. Sequencing libraries were synthesized from genomic DNA on robots according to manufacturer's protocols. Cluster generation and sequencing were performed using the manufacturer pipelines. Average sequence coverage achieved across the samples was 33.3x (range, 27.4-35.9x).

Mapping and analysis

Mapping to the human genome was performed using the BWA algorithm[39], using the BWA mem version 0.7.8. The exact genome build used was hs37d5.

Variant calling

Copy number was called using the ascatNgs[40]. The variant calling pipeline of the Cancer Genome Project, Wellcome Trust Sanger Institute was used to call somatic mutations[41]. We used the following algorithms with standard settings and no additional post-processing: CaVEMan for substitutions and the BRASS algorithm for rearrangements. For all algorithms, the parental, un-exposed samples were used as the reference samples.

Chromothripsis calling

Published chromothripsis criteria[42] were used to assess regions with complex clusters of chromothripsis. 1. Clustering of breakpoints: Applicable. Five out of nine regions with high density of rearrangements show strong clustering of rearrangement breakpoints. 2. Regularity of oscillating copy-number stages: Applicable. As opposed to “conventional chromothripsis,” copy numbers oscillate over multiple copy number states since chromothripsis takes place on chromosomes amplified through BFBs. 3. Interspersed loss and retention of heterozygosity: Applicable. Interspersed loss and retention of heterozygosity was present in multiple chromosomes with chromothripsis. 4. Prevalence of rearrangements affecting a specific haplotype: Applicable. Karyotyping analysis confirms prevalence of rearrangements on a specific haplotype. 5. Randomness of DNA segment order and fragment joins: Applicable. Rearrangements join orientations in chromothripsis regions are consistent with random draws from a uniform multinomial distribution. However, the chromothripsis events involve fairly low numbers of intra-chromosomal rearrangements, which would decrease power in finding statistical departures from a uniform multinomial distribution. 6. Ability to walk the derivative chromosome: Not applicable, as chromothripsis takes place on chromosomes with preceding duplication through BFBs. In this scenario, it would be impossible to walk the derivative chromosome[43].

Mutation calling and kataegis

Kataegis mutation clusters were detected where we observed 6 or more consecutive mutations each with an inter-mutation distance of < 1kb. This method of detection corresponds to a previously used approach[44].

Haplotype phasing of SNPs

Inspection of the variant allele frequencies (VAFs) of germline SNPs in the parental, unexposed samples revealed peaks at 1/3, 2/3 and 1, corresponding to heterozygous SNPs present on one or two copies of the triploid chromosome, as well as homozygous SNPs. Thus, we assigned SNPs to alleles based on their VAF. We defined two groups: those with variant allele frequencies (VAFs) between 0.23 and 0.43 and those with VAFs between 0.56 and 0.76. In methotrexate exposed samples we used the allelic assignments of the germline SNPs to phase copy number segments to each parental allele.

Europe PMC Funders Author Manuscripts

Simulation of DM evolution

We wondered if the dominance of multi-copy DMs is plausible when each DM is given an equal chance to randomly segregate to a daughter cell, or if an alternative mechanism, such as the frequent fusion of DMs, is responsible. To address this question, we performed *in silico* simulations of DM selection. Essentially, we allowed each cell in a population to divide depending on the number of resistance genes that it contained. A pseudocode describing the simulation procedure can be found in Supplementary Information Figure 3. The simulation was implemented in Python 2.7. In each simulation cycle and for each cell, we recorded the maximum number of resistance genes per DM. We then grouped the cells depending on their maximum DM gene copy number and evaluated the size of each group. We could then observe the growth of each cell group over the simulation cycles, which we used as a proxy for time.

Europe PMC Funders Author Manuscripts

Extended Data

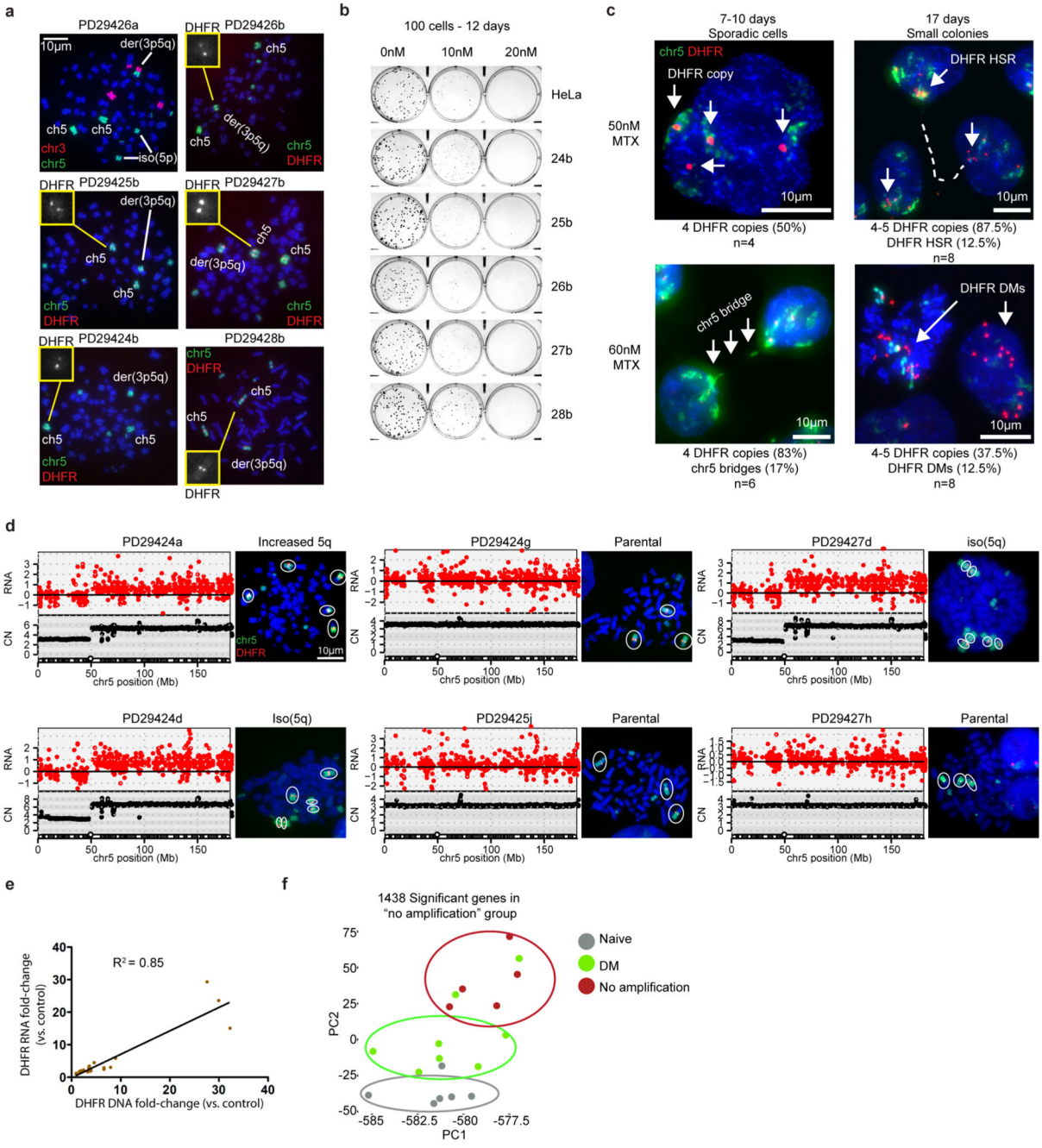

Extended Data Figure 1. Genomics and transcriptomics before and after methotrexate resistance

(**a**) Representative DNA-FISH images showing parental HeLa karyotype of chromosome 5 found in the five primary clones used in the study. The parental der(3p5q) is shown in the top left image. (**b**) Colony assay showing methotrexate sensitivity of the parental HeLa and five derivative clones. (**c**) Representative DNA-FISH images (of the indicated independent experiments n displayed below each image) of surviving cells and colonies of naïve HeLa

cells treated with methotrexate at indicated concentrations for the indicated times. Increased *DHFR* signals over wild-type (>3 signals) were frequently observed, and *DHFR* aggregates indicative of HSR formation (with chromosome 5 interphase bridge detected in some cases – outlined with white dashed line in top right image) or *DHFR*+ DMs (dispersed signal) were found in surviving colonies of 100-200 cells at day 17. (**d**) RNA expression and DNA copy number levels plotted on the linear maps of chromosome 5 of six methotrexate resistant clones with no *DHFR* amplification. Representative DNA-FISH images are displayed (of at least 10 different chromosome spreads from each clone). (**e**) Linear regression comparing DNA copy number and RNA expression levels of *DHFR* in methotrexate resistant HeLa clones. (**f**) Principal component analysis (PCA) of naïve and resistant HeLa clones (with DMs or without *DHFR* amplification).

Europe PMC Funders Author Manuscripts

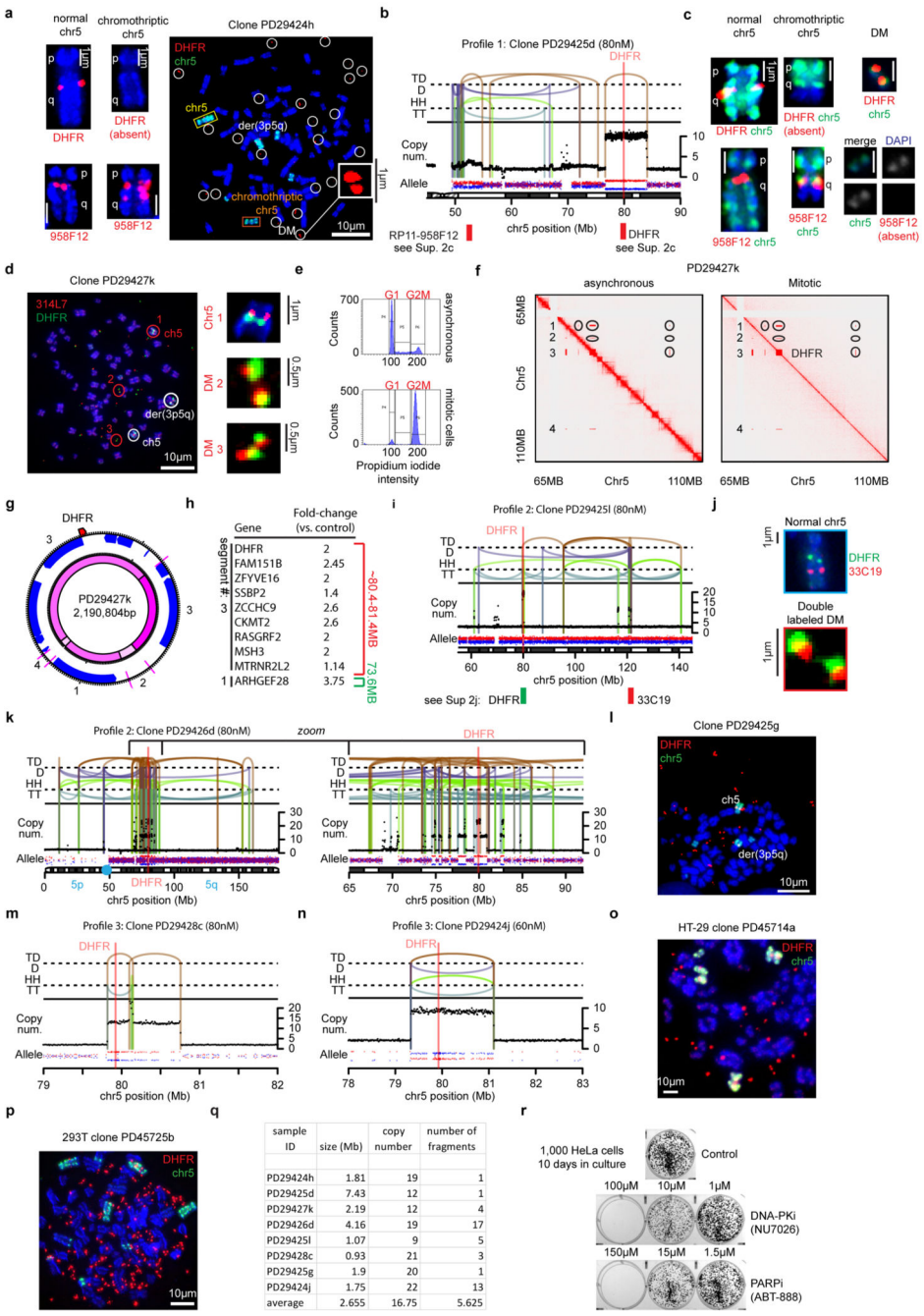

Extended Data Figure 2. Formation of DMs through chromothripsis in methotrexate resistant cells

(**a**) Representative DNA-FISH of metaphase spread prepared from clone PD29424h showing *DHFR* amplified in DMs (marked with white circles). Alignment of the normal chromosome 5 (*DHFR*+) and shorter chromothriptic chromosome 5 (*DHFR*-) is presented. Representative DNA-FISH from a metaphase spreads hybridized with chromosome 5 paint probe (green) and BAC probe (RP11-958F12, red, ~30Mb away from DHFR) found on both the normal chromosome 5 (single location) and shorter chromothriptic chromosome 5 (multiple

dispersed locations) is also presented (**b, I, k, m-n**) Copy number, allelic ratio, and structural variation profiles of indicated samples. (**c**) Representative FISH images from clone PD29425d showing a normal chromosome 5 (*DHFR*+, RP11-958F12 positive), a shorter chromothriptic chromosome 5 (*DHFR*-, RP11-958F12 positive), and a DM (*DHFR*+, RP11-958F12 negative). See panel **b** for BAC probe target. (**d**) Representative DNA-FISH image of metaphase spreads prepared from clone PD29427k and hybridized with BAC RP11-314L7 (labels fragment #1 of the DM as shown in Figure 1d) and *DHFR* locus probes. Insets show the co-localization of the non-contiguous genomic locations within the DMs. (**e**) Representative FACS analysis using propidium iodide staining showing cell cycle distribution in asynchronized and mitotic clones prepared for Hi-C experiments. For gating strategy see Supplementary Information Figure 2. (**f**) *In situ* Hi-C map of chromosome 5 (65-110Mb) of asynchronized and mitotic cells from methotrexate resistant clone PD29427k. Interactions between distant chromosome locations (preserved also in the mitotic sample where topologically associated domains are erased) are circled in black (above the diagonal red line) and presented natively (below the line). (**g**) Reconstruction of the circular map of the DM present in clone PD29427k. Numbers represent the four DM segments appearing in panel **f** (notice that segment 3 is rearranged). (**h**) List of the genes found on the DM (with RNA expression relative to naïve HeLa cells). Numbers represent the four DM segments appearing in panel **f**. (**j**) Representative DNA-FISH from clone PD29425l showing co-localization of *DHFR* (green) and BAC 33C19 probes signals. See panel **i** for BAC probe target. (**l**) Representative DNA-FISH image of metaphase spreads prepared from clone PD29425g hybridized with chromosome 5 paint (green) and *DHFR* locus (red) probes. Inset shows the *DHFR* positive DM. Notice only one chromosome 5 and one der(3p5q) are present. (**o-p**) Representative DNA-FISH image of metaphase spreads prepared from clones PD45714a (**o**) and PD45725b (**p**) hybridized with chromosome 5 paint (green) and *DHFR* locus (red) probes showing DHFR amplification in DMs. (**q**) List of DM+ HeLa clones showing size, copy number, and number of non-contiguous fragments. (**r**) Colony assay of naïve HeLa cells treated with DNA repair inhibitors (control – untreated). Images are representative of two independent experiments.

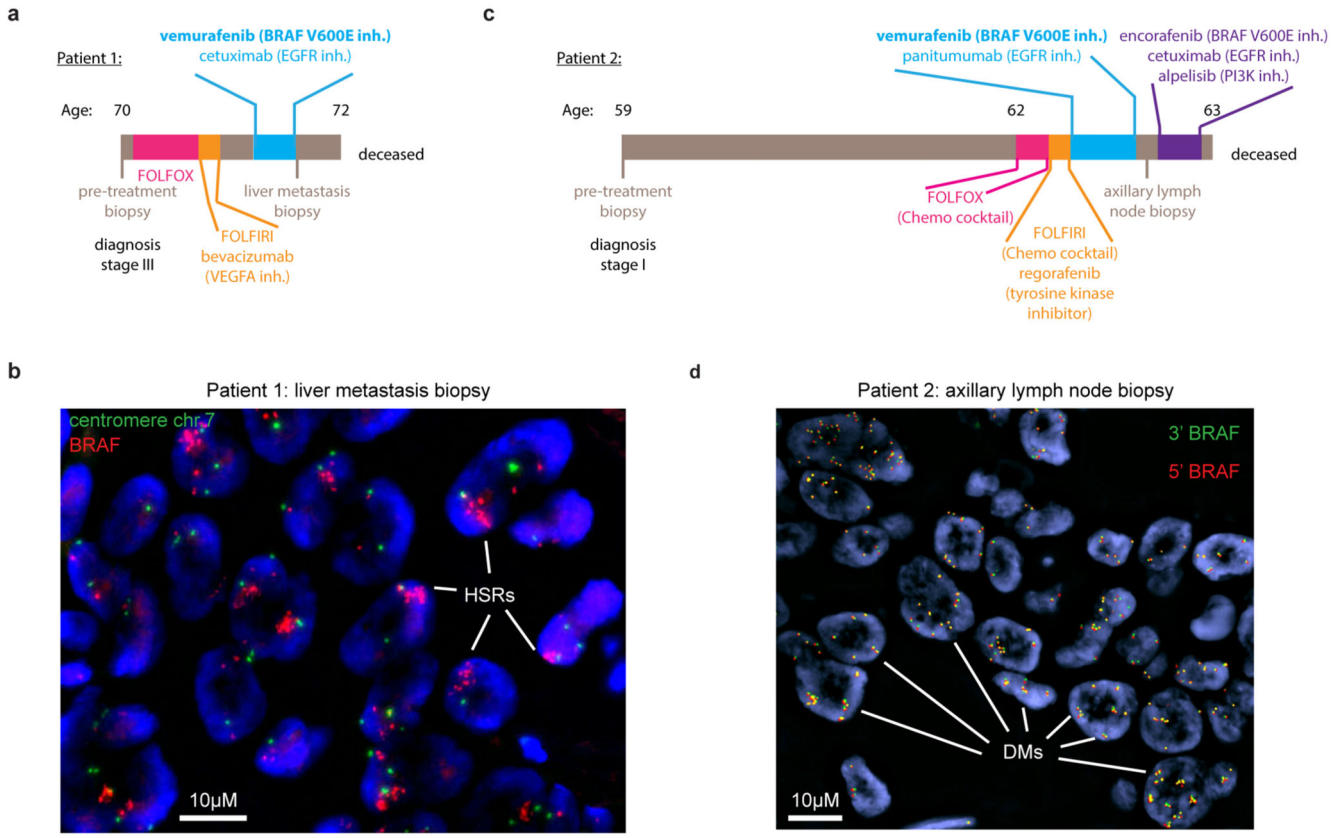

Extended Data Figure 3. BRAF^{V600E} amplification in drug resistant colorectal cancer patients

(**a, c**) Treatment and biopsies collection timeline of colorectal cancer patient 1 and 2. (**b, d**) Representative FISH images (of entire section stained) showing BRAF amplification in biopsies from post-treatment biopsies from patients 1 and 2. Probes used are listed in the methods section.

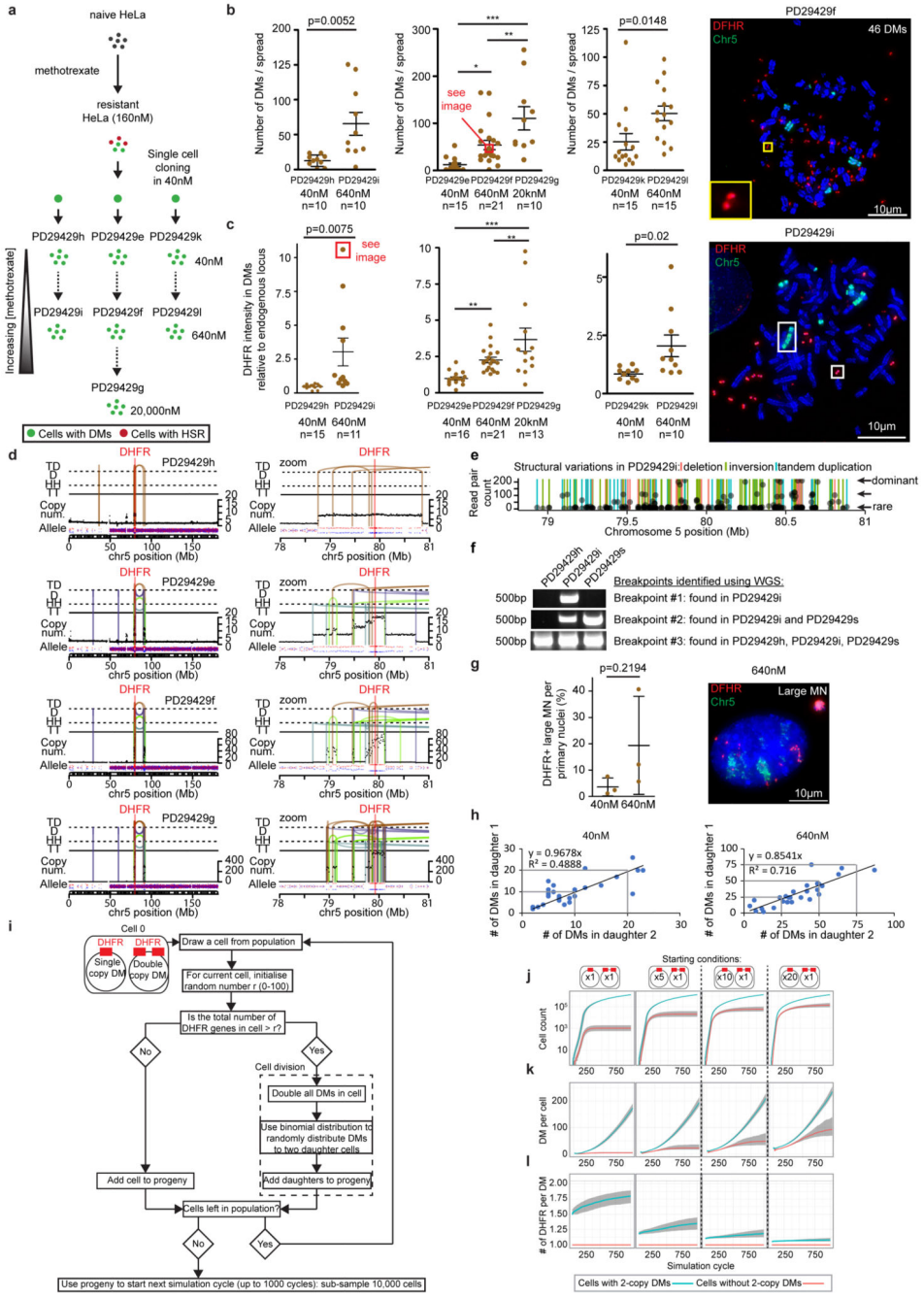

Extended Data Figure 4. DMs are numerically and structurally unstable

(**a**) Strategy used to isolate DM or HSR positive clones from a heterogeneous population of methotrexate resistant HeLa cells. (**b**) Left: Average number of *DHFR*+ DMs in three clones derived from a methotrexate resistant HeLa population was determined using DNA-FISH. Analyses with indicated p-values above plots were performed using Student t-test. *p<0.05, **p<0.01, ***p<0.001 are p-values calculated using one-way ANOVA. Error bars represent mean±s.e.m., number of spreads examined for each condition is written below each graph. Right: Representative DNA-FISH image of metaphase spreads from clone PD29429f

Europe PMC Funders Author Manuscripts

Europe PMC Funders Author Manuscripts

(640nM) containing 46 *DHFR*+ DMs as determined by DNA-FISH. Inset shows a representative DHFR positive DM. (**c**) Average intensity of *DHFR* signal in DMs relative to the intensity of the endogenous *DHFR* signal on chromosome 5 from the same spread, as determined by DNA-FISH using a probe (RP11-90A9) specific for the *DHFR* locus. Analyses with indicated p-values above plots were performed using Student t-test. **p<0.01 and ***p<0.001 are p-values calculated using one-way ANOVA. Error bars represent mean ± s.e.m. Representative DNA-FISH image of chromosome spread from which insets are shown in Figure 2b is presented. (**d**) Copy number, allelic ratio, and structural variation profiles of indicated samples. (**e**) Read counts in structural variation breakpoints in sample PD29429i showing potential different DM subspecies forming through chromothripsis (**f**) Breakpoint PCR using primers specific for three different rearrangements detected using WGS. For gel source data, see Supplementary Information Figure 1. (**g**) Percentage of DM-positive cells exposed to low or high methotrexate concentrations with large micronuclei, as determined by DNA-FISH. Results represent an average of 3 clones per methotrexate concentration (as seen in Extended Data Fig. 4a), error bars represent mean ± SD. Representative DNA-FISH image of a cell with a large micronucleus is provided. 40nM: n = 147, 130, 98; 640nM: n = 74, 216, 133. (**h**) Analysis of DM inheritance to two daughter cells after one cell division. Cells were seeded at low dilution and 24 hours later DNA-FISH on interphase daughter cells from PD29429h (40nM) or PD29429i (640nM) was performed using a DHFR probe. DM numbers in each daughter cell were counted and plotted on an x-y plot (n = 54 daughters per condition). (**i**) Schematic explaining the steps of a simulation testing the effect of harboring DMs with more than one DHFR gene. (**j-l**) In-silico simulation showing that cells containing a 2-copy *DHFR* DM have a selection advantage (**i**), with increased DM content (**j**), and that 2-copy *DHFR* DMs are selected over DMs with a single copy of *DHFR* (**k**). Plotted is the median and first and third quartile (grey ribbon). For simulation pseudocode see Supplementary Information Figure 3.

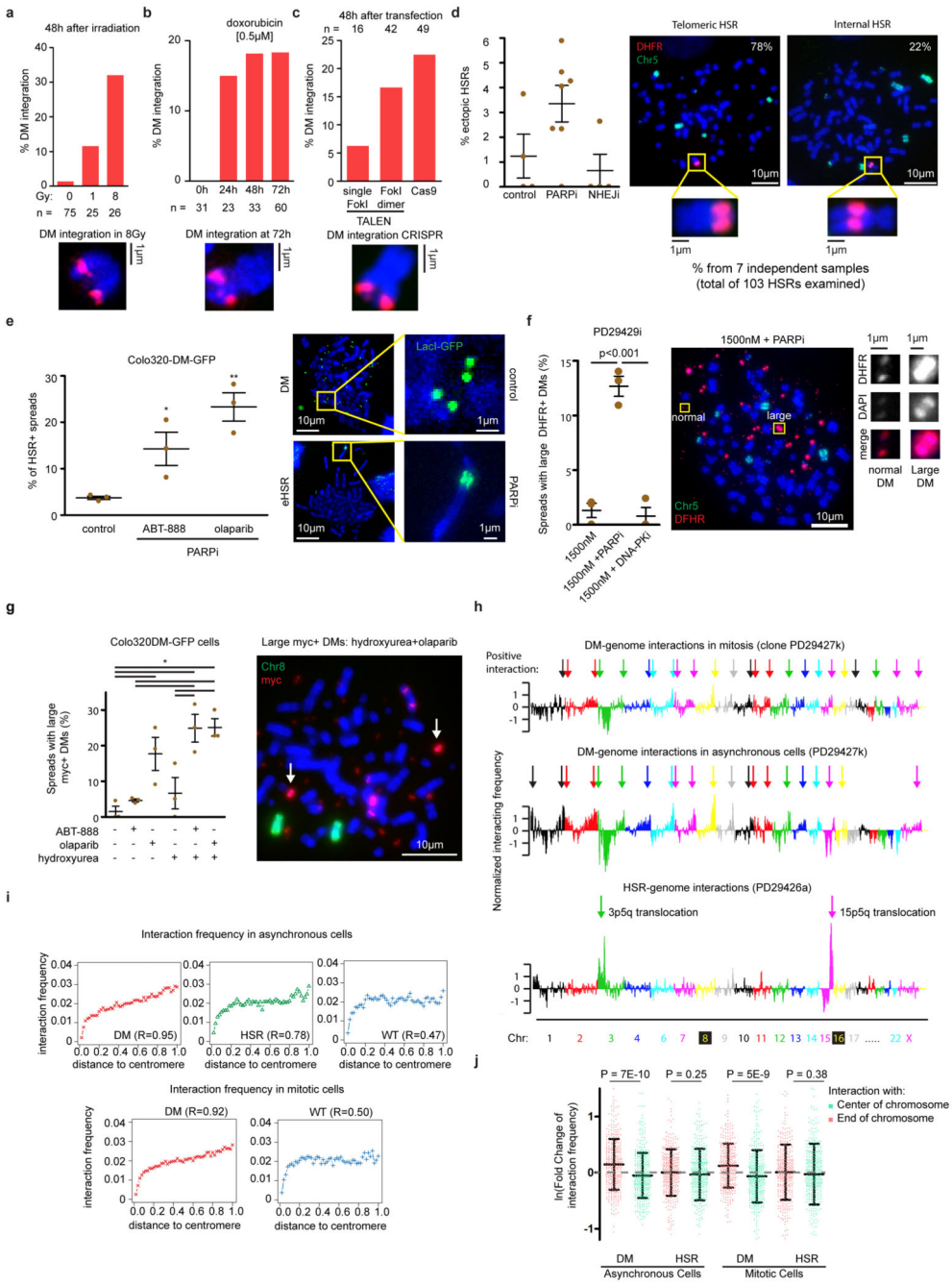

Extended Data Figure 5. DMs integrate into ectopic chromosomes following DNA damage

(**a-c**) Percentage of DM integration as detected using DNA-FISH with probes against chromosome 5 (green) and *DHFR* (red) in clone PD29429i after ionizing irradiation (**a**), doxorubicin (**b**), or transfection with nucleases specific for a region near the *DHFR* locus (**c**). Representative images of DNA-FISH of DMs integrated into ectopic chromosomes are presented below each graph. (**d**) Percentage of ectopic HSRs detected in DM-positive clones treated with increased methotrexate concentration (x2.5 fold higher) with or without (control, 4 clones) the addition of ABT-888 (PARPi, 7 clones) and NU7026 (NHEJi, 4

Europe PMC Funders Author Manuscripts

Europe PMC Funders Author Manuscripts

clones) for 3 weeks. Means ± s.e.m. are presented. control: n = 107, 96, 46, 164; PARPi: n = 67, 247, 94, 128, 17, 130; NHEJi: n = 51, 45, 28, 38. Representative FISH images of ectopic HSRs at the end of chromosome (78% of the cases) or in the middle of chromosomes (22% of the cases) are presented. (**e**) Percentage of GFP+ HSRs detected in colo320DM-GFP cell line treated with DMSO (control) or with ABT-888 (PARPi) or olaparib (PARPi) for 2 weeks. Means ± s.e.m. of three independent experiments are shown. p-values *p<0.05 and **p<0.001 calculated using one-way ANOVA are presented. control: n = 26, 47, 33; ABT-888: n = 42, 44, 37; Olaparib: n = 29, 32, 34. Representative fluorescent images of GFP+ DMs (from control) and GFP+ HSRs (from PARPi treated cells) are presented. (**f**) Percentage of chromosome spreads in which large *DHFR*+ DMs were detected using DNA-FISH when PD29429i was exposed to 1500nM methotrexate only (control) or with addition of 15μM ABT-888 (PARPi) or 10μM NU7026 (DNA-PKi) for 3 weeks. Means ±s.e.m of three independent experiments are presented. * p-value < 0.001 calculated using one-way ANOVA and Tukey's Multiple Comparison Test. Number of spreads scored per condition/ experiment: 1500nM MTX (52, 53, 49), 1500nM MTX + ABT-888 (50, 76, 55), 1500nM MTX + NU7026 (57, 16, 42). Representative image (of three independent experiments as shown in the plot to the left) of a chromosome spread containing multiple normal sized and large DMs is presented. (**g**) Percentage of chromosome spreads in which large myc+ DMs were detected using DNA-FISH in colo320DM-GFP cells with indicated types of treatment for 2 weeks (DMSO served as control, PARP inhibitors used were 15μM ABT-888 and 10μM Olaparib, hydroxyurea used at 100μM). Representative image of a chromosome spread containing multiple normal sized and large DMs (white arrows) is presented. Means ± s.e.m of three independent experiments with *p<0.05 calculated using one-way ANOVA are presented. control: n = 22, 22, 21; ABT-888: n = 26, 19, 21; Olaparib: n = 20, 22, 21; hydroxyurea: n = 20, 22, 20; hydroxyurea+ABT-888: n = 19, 22, 24; hydroxyurea+Olaparib: n = 20, 22, 22. (**h**) Quantification of the interaction frequency between DM or HSR sequences and the rest of the genome in mitotic or asynchronous cells. Linear chromosome maps (chromosomes 1-X, excluding chromosome 5) are presented from beginning to end (p arm to q arm direction), and the normalized interaction frequency is presented. (**i**) Interaction frequency as a function of distance from the centromere (R - pearson correlation). (**j**) Fold-change (relative to cells with no amplification) of *DHFR* sequences interaction in DM+ and HSR+ with center of chromosomes (50% of sequences in chromosome center) and with chromosome ends (25% of sequences in each chromosome end). p-values calculated using two-sided paired t-test.

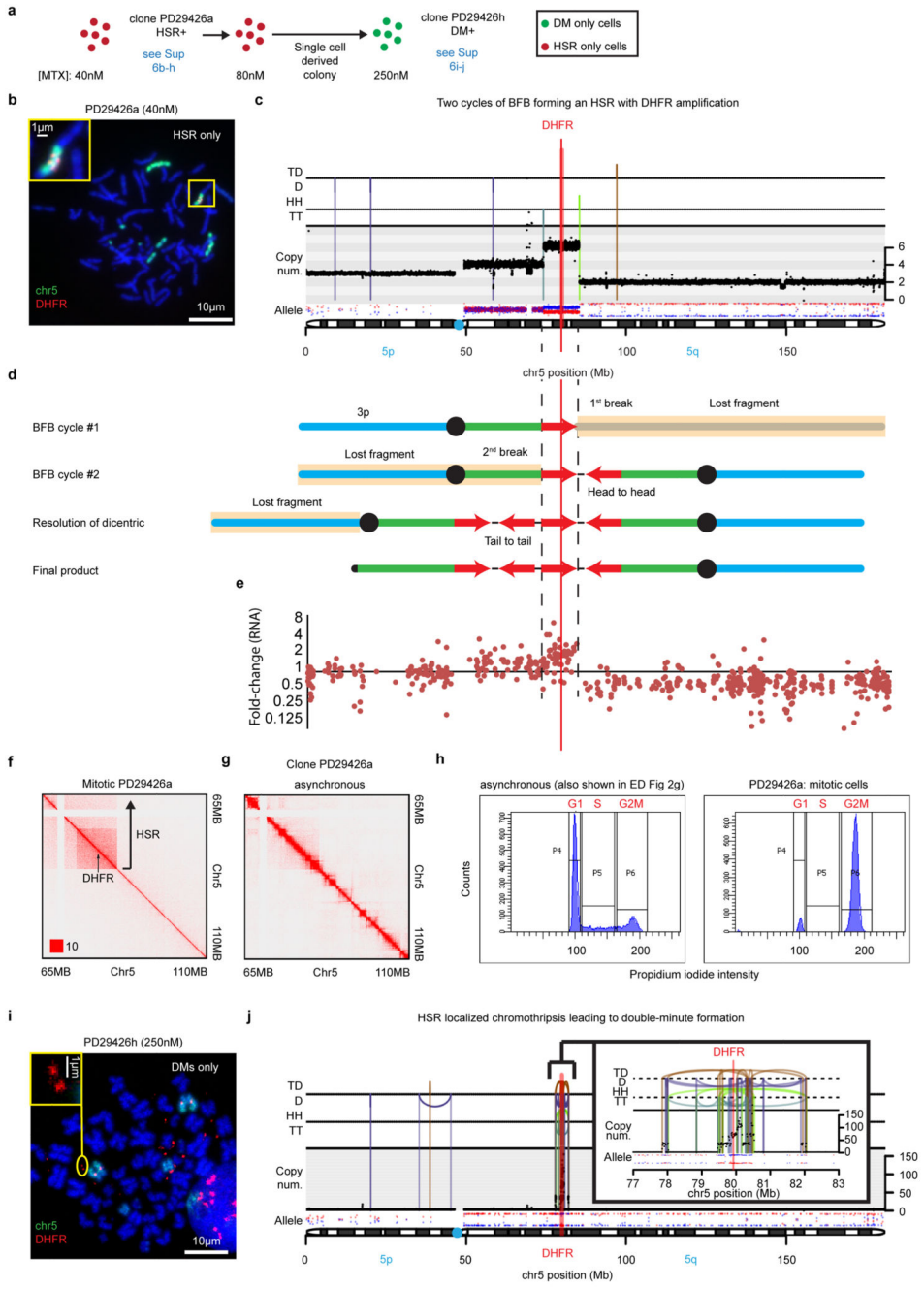

Extended Data Figure 6. Increased selective pressure drives the transition of intra- to extra-chromosome amplification through chromothripsis

(**a**) Experimental outline of a parental HSR+ clone treated with increasing methotrexate concentrations. (**b**) Representative FISH image of 23 metaphase spreads prepared from the methotrexate resistant HSR+ clone PD29426a hybridized with chromosome 5 paint (green) and *DHFR* locus (red) probes. Inset shows the *DHFR* repeat located on the 5q arm of the derivative 3p5q chromosome. (**c**) DNA copy number, rearrangement, and allelic ratio profile of clone PD29426a showing two copy number jumps flanked by head-to-head and tail-to-tail

Europe PMC Funders Author Manuscripts

inversions corresponding to two BFB cycles. (**d**) Schematic depicting the order of events during the two break-fusion-bridge (BFB) cycles that led to the formation of the HSR in clone PD29426a. (**e**) RNA expression presented on the linear chromosome 5 map showing increased gene expression from the HSR region. (**f**) *In situ* Hi-C map of chromosome 5 (65-110Mb) of mitotic cells from methotrexate resistant clone PD29426a, showing the HSR in which there is higher interaction within the regions with copy number jumps. (**g**) *In Situ* Hi-C map of chromosome 5 (65-110Mb) of asynchronized cells from HSR+ clone PD29426a. TADs are visible throughout this region and increased interactions are observed in the HSR region (increased red coloration, top left quadrant). (**h**) Cell cycle analysis using propidium iodide staining showing cell cycle distribution in asynchronized and mitotic cells of clone PD29426a. For gating strategy see Supplementary Information Figure 2. (**i**) Representative FISH image (of two independent clones, total of 26 spreads imaged) of metaphase spreads prepared from a DM subclone (PD29426h) derived from the HSR+ clone PD29426a. Spreads were hybridized with chromosome 5 paint (green) and *DHFR* locus (red) probes. Inset shows the *DHFR* positive DMs. (**j**) DNA copy number, rearrangement, and allelic ratio profile of clone PD29426h. The DM is composed of fragments with varying copy number states derived from the original HSR region, connected by multiple rearrangements.

Europe PMC Funders Author Manuscripts

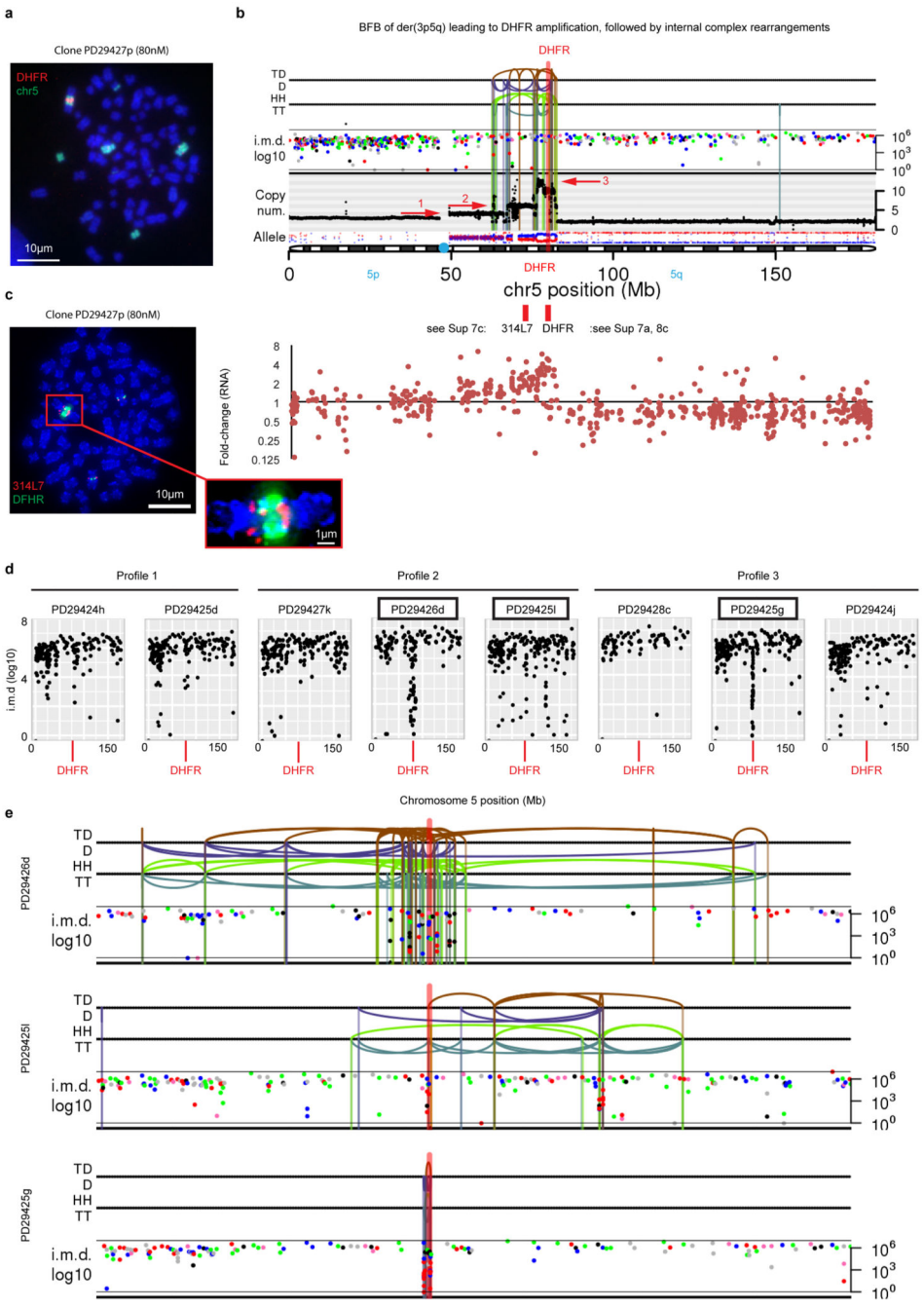

Extended Data Figure 7. Chromothripsis and kataegis in gene amplification

(**a**) Representative FISH image (of 12 spreads imaged) of metaphase spreads prepared from clone PD29427p and hybridized with chromosome 5 paint (green) and *DHFR* locus probes, revealing the existence of a DHFR+ HSR. (**b**) Top: Copy number profile of a methotrexate resistant clone (PD29427p) presenting an HSR profile resulting from 3 BFB cycles with overlaid complex rearrangements. Rearrangements are presented on top: TD – tandem duplication, D – deletion, HH – head-to-head inversion, TT – tail-to-tail inversion. Inter-mutation distance (i.m.d) and allelic ratio (bottom, blue/red dots) are also presented. Bottom:

RNA expression profile of clone PD29427p, relative to control naïve HeLa cells, presented on the linear map of chromosome 5 and matching the DNA copy number plotted above. (**c**) Representative FISH image (of 6 spreads imaged) of metaphase spreads prepared from clone PD29427p and hybridized with chromosome 5 paint (green) and BAC probe 314L7 (see chromosomal location indicated in panel **b**) probes. Inset shows probe 314L7 signal is flanking the DHFR signal within the HSR. (**d**) Rainfall plots showing the inter-mutation distance (i.m.d.) within chromosome 5 of each DM clone. (**e**) Structural variations and inter-mutation distance (i.m.d.) of three kataegis positive DM clones.

Europe PMC Funders Author Manuscripts

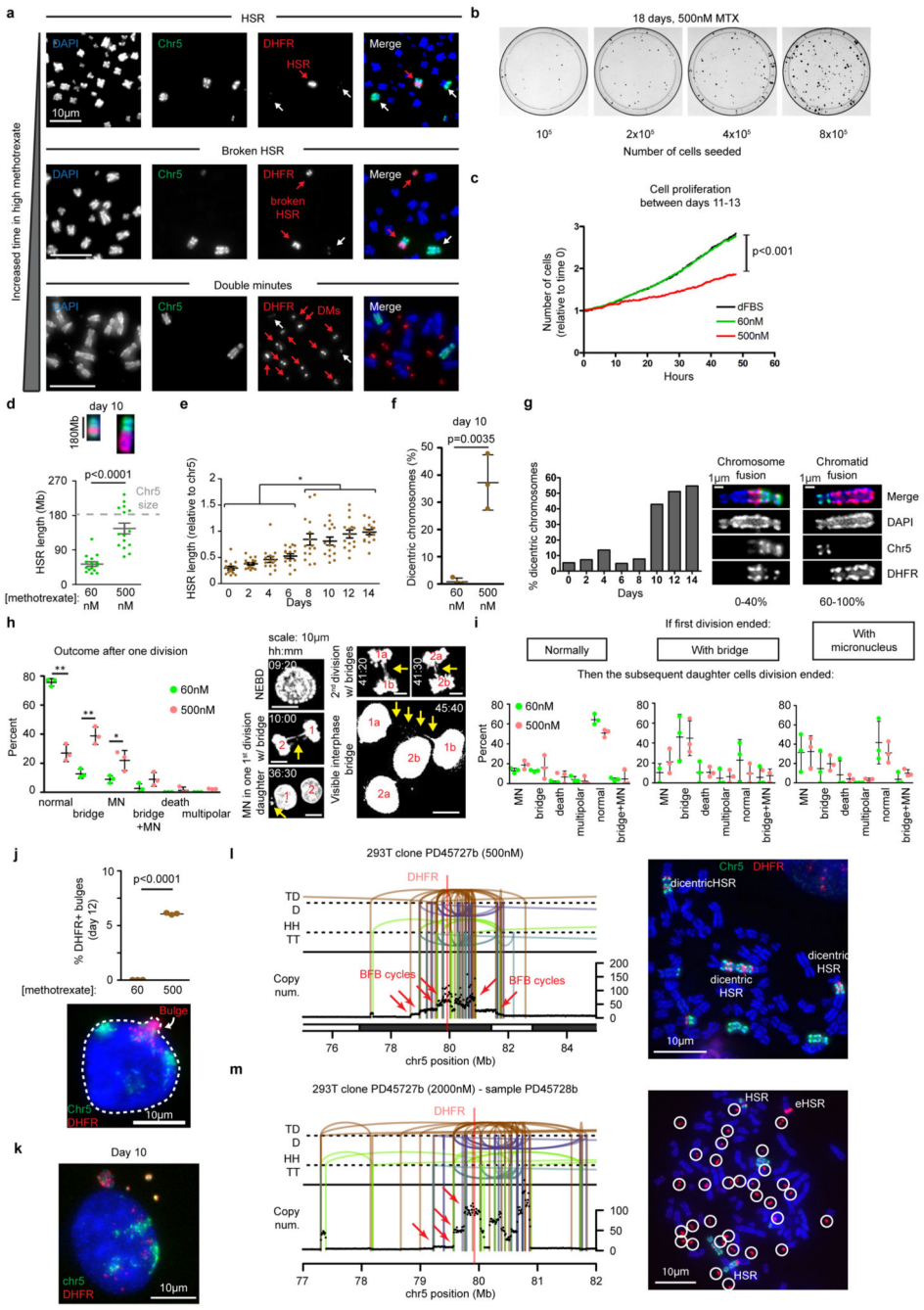

Extended Data Figure 8. Characterization of steps leading to HSR fragmentation and DM formation

(**a**) Representative FISH images (of 464 spreads imaged from 8 different timepoints as shown in Figure 4a) showing chromosome 5 (green) and *DHFR* (red) probes in HSR+ clone PD29428e at basal methotrexate concentration (60nM, top), and following treatment with increased methotrexate (500nM, middle and bottom) in which HSR fragments of variable sizes and DMs can be detected. (**b**) Colony assay of clone PD29428e (HSR+) resistant to 60nM and treated with 500nM methotrexate. Numbers of cells seeded are indicated and

Europe PMC Funders Author Manuscripts

colonies were fixed and stained at day 18. (**c**) Number of cells counted (automatically) using the CQ1 microscope in 10 minutes interval during 48 hours of filming of PD29428e cells treated with 60nM or 500nM or without (dFBS) methotrexate. Cell numbers were normalized to the initial number present at time point 0. P-value calculated using one-way ANOVA. (**d**) Measurement of the HSR length in clone PD29428e after ten days of exposure to higher methotrexate concentration. The length of the HSR was normalized to the length of the normal chromosome 5 from the same spread. Mean ± s.e.m. of n=15 per group and p-value calculated using two-tailed t-test are presented. Insets showing length of the HSR at day 10 after exposure to basal (left) or increased (right) methotrexate concentrations (scale is 180MB, equivalent to chromosome 5 size). (**e**) Measurement of the HSR length in clone PD29428e during two-week exposure to higher methotrexate concentration. The length of the HSR was normalized to the length of the normal chromosome 5 from the same spread. Means ±s.e.m of 15 HSR lengths per each timepoint (except day 14 – 16 HSRs scored). p-values calculated using one-way ANOVA and * denotes significant (range of $p<0.05$-0.001) change in HSR length between each point of 8-14 days and each point of 0-6 days. (**f**) Percentage of spreads containing dicentric HSR+ chromosomes in clone PD29428e exposed to basal or increased methotrexate concentration for 10 days. Mean ± SD of three independent experiments (60nM: n = 42, 30, 33; 500nM: 23, 33, 29) and p-value calculated using two-tailed t-test are presented. (**g**) Percentage of spreads containing dicentric HSR+ chromosomes in clone PD29428e after increasing methotrexate concentration for the indicated times. day 0: n = 98; day 2: n = 41; day 4: n = 39; day 6: n = 63; day 8: n = 53; day 10: n = 55; day 12: n = 66; day 14: n = 123. Inset shows representative image (from 538 spreads imaged) of a chromatid-type dicentric chromosome with one fused end, and chromosome type fusion with two distinct centromeres. Percentages indicate frequency range of each dicentric type throughout the two-week experiment. (**h**) Abnormalities identified in PD29428e cells treated without or with increased methotrexate concentration (60nM and 500nM, respectively) for 11 days during 48 hours filming. Mean ±S.D. of three independent experiments and p-values (*$p<0.01$ and *$p<0.001$) calculated using two-way ANOVA are presented. Division scored: 60nM: n = 115, 108, 95; 500nM: n = 51, 50, 42. Bridges (anaphase bridges), micronuclei (MN), bridges+MN, death, and multipolar divisions were scored. Insets from Supplementary Video 1 showing anaphase bridges, micronuclei, and also interphase bridges are presented. (**i**) Analysis as performed in (h) looking at events occurring during the division of the daughter cells generated from the parental cells scored in (**h**). Division scored: 60nM: n = 100, 90, 66; 500nM: n = 85, 76, 66 (**j**) Top: Percentage of nuclei presenting *DHFR*+ nuclear bulges indicative of bridge rupture in PD29428e HSR+ clone treated with increased methotrexate (500nM) over the course of 12 days. Mean ± SD of three independent experiments (60nM: n = 144, 221, 204; 500nM: n = 163, 218, 214) and p-value calculated using two-tailed t-test are presented. Bottom: Representative image of *DHFR*+ (red) labeled nuclear bulge. (**k**) Representative image of the data in Fig. 4d. (**l**) Copy number profile of a methotrexate resistant clone (PD45727b) presenting an HSR profile resulting from multiple BFB cycles (marked with red arrows) with overlaid complex rearrangements. A representative DNA-FISH image (of 20 spreads imaged) showing dicentric HSRs is presented. DMs were observed in low frequency under this condition. (**m**) Copy number profile of clone PD45727b subjected to increased methotrexate concentration (sample PD45728b) presenting additional rearrangements and formation of multiple DMs

(as seen in the representative DNA-FISH image from 10 spreads imaged, white circles). TD – tandem duplication, D – deletion, HH – head-to-head inversion, TT – tail-to-tail inversion.

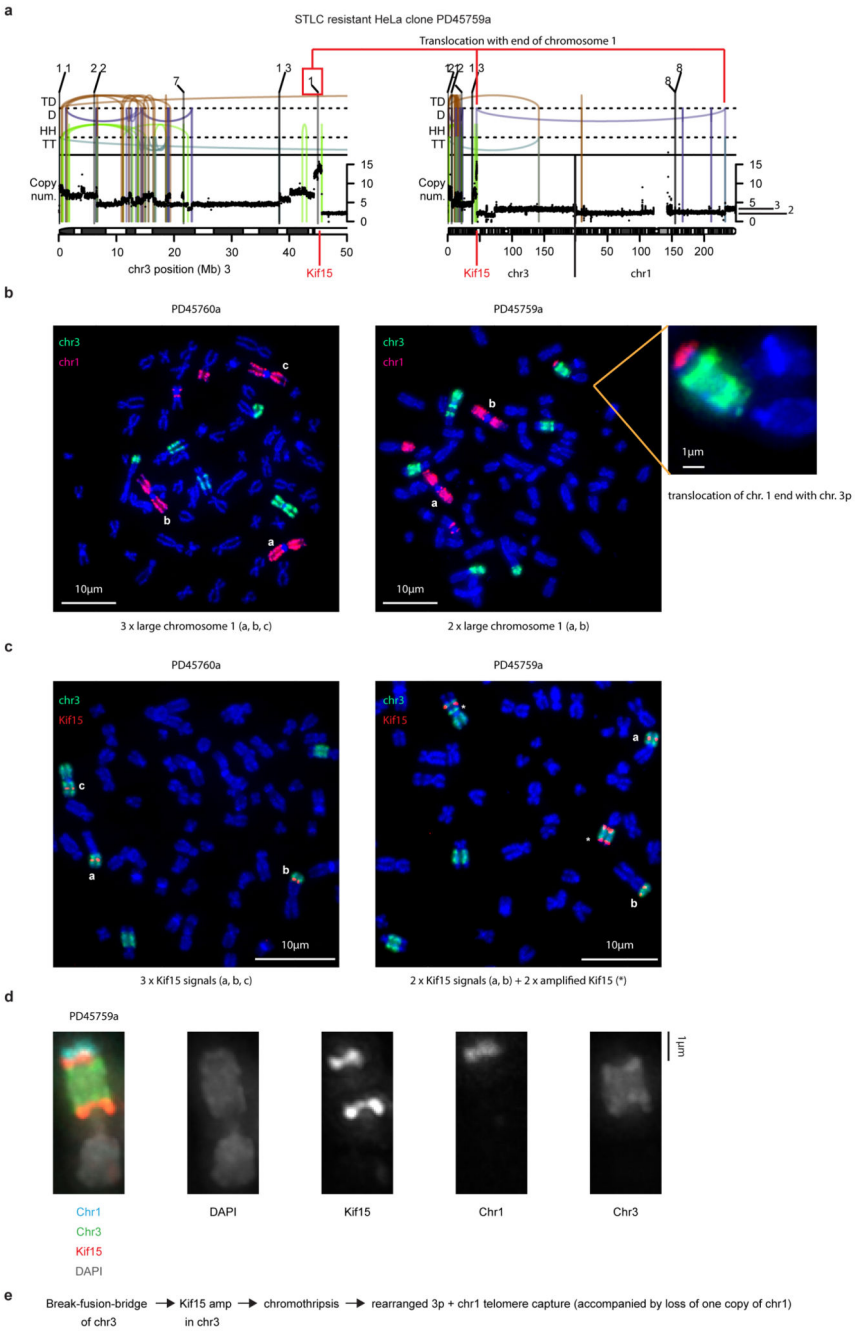

Extended Data Figure 9. Chromothripsis drives resolution of Kif15 intra-chromosomal amplification through telomere capture

(**a**) Copy number profile of chromosome 3 showing a rearranged 3p region with Kif15 amplification (copy number = 15) and a translocation of a telomeric fragment from a lost chromosome 1. (**b**) Representative DNA FISH images (of 33 spreads imaged) from STLC resistant clones with (PD45759a) or without (PD45760a) Kif15 amplification showing the

Europe PMC Funders Author Manuscripts

translocation of the telomeric chromosome 1 fragment to the end of a chromosome 3 arm. (**c**) Representative DNA FISH images (of 20 spreads imaged) for chromosome 3 (green) and Kif15 (RP11-659N22, red) showing normal Kif15 in PD45760a (STLC resistant without Kif15 amplification, 3 Kif15 copies labeled with “a”, “b”, and “c”) and in PD45759a (STLC resistant with Kif15 amplification found on two rearranged chromosomes marked with “*” and originating from chromosome “c” as seen in PD45760a). (**d**) Representative DNA FISH image (from 25 spreads imaged) showing from PD45759a showing the rearranged chromosome containing Kif15 amplification and telomeric region of chromosome 1 at the tip of the chromosome. (**e**) Proposed order of events leading to Kif15 amplification and resolution of the dicentric state through a chromothriptic event.

Europe PMC Funders Author Manuscripts

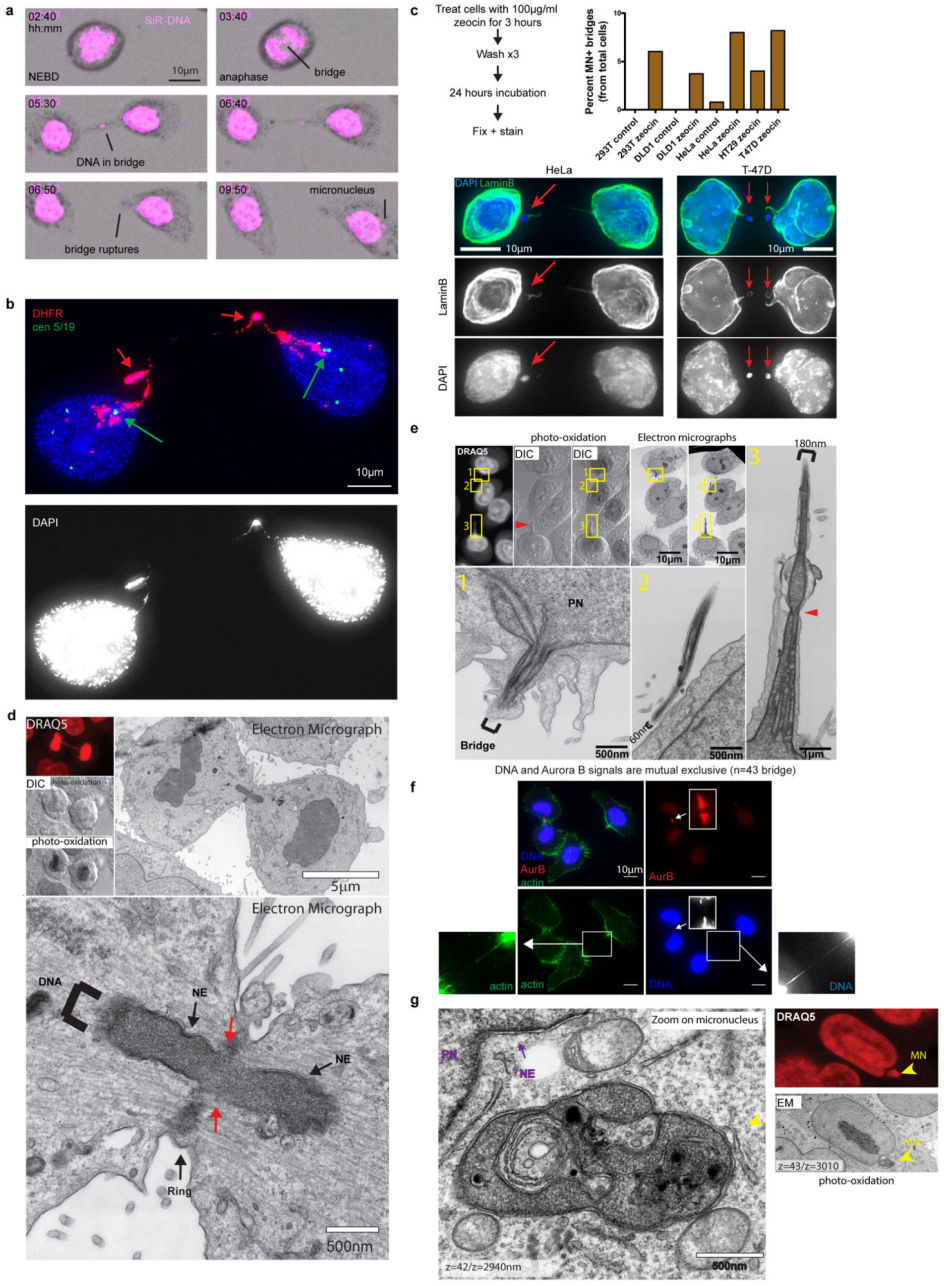

Extended Data Figure 10. Structure of the interphase chromosome bridge

(**a**) Snapshots from live cell imaging (Supplementary Video 2) of PD29428e cells exposed to increased methotrexate concentration (500nM) for 11 days, labeled with SiR-DNA label, and filmed for 48 hours (of 944 cell divisions filmed, as shown in Extended Data Figure 8h-i). Frames are at 10-minute intervals. An initial DNA+ bridge forms from which a DNA fragments is maintained as a micronucleus following bridge rupture. (**b**) Representative image of PD29428e cells exposed to increased methotrexate concentration (500nM) for 10 days and analyzed using DNA FISH probes for chromosome 5 centromere (green) and

Europe PMC Funders Author Manuscripts

DHFR (red), showing micronuclei within interphase DNA bridges (representative of 34 bridges) (**c**) Immunofluorescent image analysis of zeocin treated cancer cell lines showing formation of micronuclei within interphase DNA bridges (representative images of 85 bridges with micronuclei from the four cell lines tested. Number of cells scored: 293T control: n = 99; 293T zeocin: n = 116; DLD1 control: n = 88; DLD1 zeocin: n = 107; HeLa control: n = 126; HeLa zeocin: n = 412; HT29 zeocin: n = 25; T47d zeocin: n = 73). (**d-e**), correlative light and electron microscopy (CLEM) images (of a total of 5 images taken) of an anaphase bridge (**d**, red arrow marks aberrant nuclear envelope at midbody region) and an interphase bridge (**e**, red arrow marks constriction in DNA bridge at midbody site). NE – nuclear envelope. (**f**) Representative immunofluorescence images (of 43 different bridges) showing AuroraB localization in interphase DNA bridges. (**g**) Correlative light and electron microscopy (CLEM) of an abnormally shaped micronucleus found in PD29428e cells exposed to increased methotrexate concentration (500nM) for 10 days in which micronuclei form following interphase bridge rupture (representative of 2 micronuclei imaged).

Europe PMC Funders Author Manuscripts

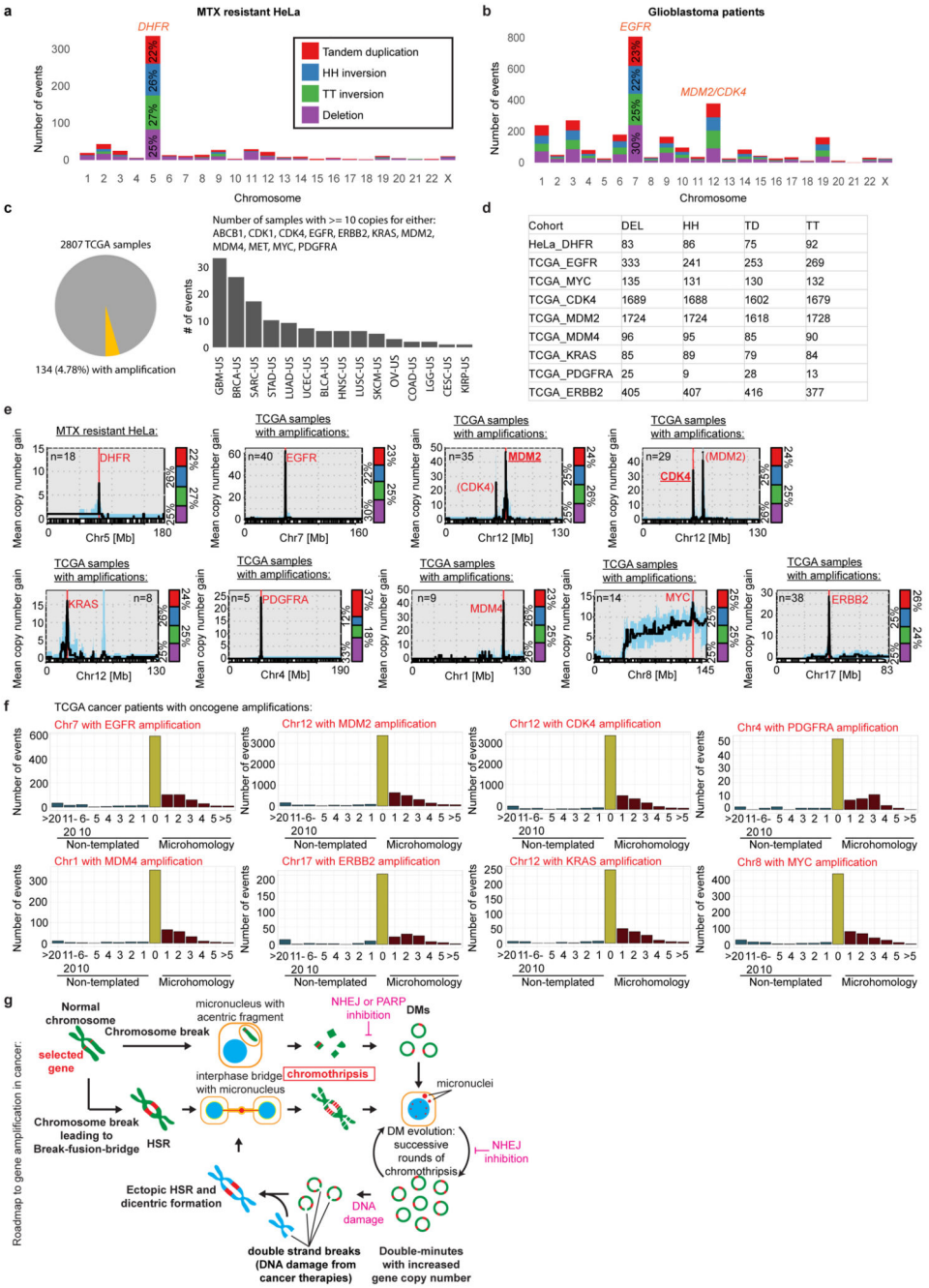

Cohort	DEL	HH	TD	TT
HeLa_DHFR	83	86	75	92
TCGA_EGFR	333	241	253	269
TCGA_MYC	135	131	130	132
TCGA_CDK4	1689	1688	1602	1679
TCGA_MDM2	1724	1724	1618	1728
TCGA_MDM4	96	95	85	90
TCGA_KRAS	85	89	79	84
TCGA_PDGFRA	25	9	28	13
TCGA_ERBB2	405	407	416	377

Extended Data Figure 11. Similarities between DHFR and oncogene amplifications

(**a**-**b**) Summary of the overall structural variant events found across all samples analyzed in the methotrexate resistant HeLa cohort (**a**, 18 clones) and in glioblastoma cancer patients from the TCGA database (**b**, 41 patients). (**c**) Amplifications (>= 10 copy numbers) of either of 11 indicated genes in patients found in the TCGA database. (**d**) Distribution of rearrangements in chromosomes containing specific amplifications. Near equal distribution of rearrangements suggest events are random as expected in chromothripsis. TD – tandem duplication, D – deletion, HH – head-to-head inversion, TT – tail-to-tail inversion. (**e**) Copy

number plots showing the mean copy number gain presented on the linear chromosome map in methotrexate resistant HeLa cells (chromosome 5) and TCGA samples presenting oncogene amplifications. The percentage of each type of rearrangement found in chromosomes with amplifications is presented. Red – tandem duplications, Blue – head-head inversions, Green – tail-tail inversions, Purple – deletions. (**f**) Microhomology (red), non-templated (teal) sequences, or direct end-joining (yellow), found at breakpoints in chromosomes with specific oncogene amplifications from TCGA patients. The number of homologous or non-homologous bases at breakpoints are shown on the x-axis. The number of breakpoints showing each kind of junction is shown on the y-axis. (**g**) Schematic illustrating a roadmap to gene amplification in cancer cells.

Supplementary Material

Refer to Web version on PubMed Central for supplementary material.

Acknowledgements

This work was funded by grants from the US National Institutes of Health (R35 GM122476 to D.W.C.), Wellcome Trust (WT088340MA to P.J.C.), US National Institutes of Health (K99 CA218871 to P.L.), the Swiss National Science Foundation (P2SKP3-171753 to S.F.B), Ludwig Institute for Cancer Research (D.W.C. and B.R.), the MSK Cancer Center Core Grant from the NIH (P30 CA 008748 to R.Y.), the National Institute of General Medical Sciences (P41GM103412, R24GM137200 to M.H.E), and the High End Instrumentation Award (S10OD021784 to M.H.E). D.W.C. and B.R. receive salary support from the Ludwig Institute for Cancer Research. We thank Andrew Shiau for providing access to the CQ1 spinning disk confocal system. We thank Noriaki Shimizu (Hiroshima University, Japan) for providing the Colo320-DM-GFP cell line.

Data availability

Paired-end whole genome sequencing data is available at ENA (European Nucleotide Archive), accession number ERP107458 https://www.ebi.ac.uk/ena/data/view/PRJEB25535

In-situ Hi-C sequencing data is available at GEO (Gene Expression Omnibus), accession number GSE119825, using the following link: https://www.ncbi.nlm.nih.gov/geo/query/acc.cgi?acc=GSE119825

RNA sequencing data is available at GEO (Gene Expression Omnibus), accession number GSE119979, using the following link: https://www.ncbi.nlm.nih.gov/geo/query/acc.cgi?acc=GSE119979

Source data are provided with this manuscript.

TCGA database can be accessed in https://portal.gdc.cancer.gov/.

Code Availability

A pseudocode of the simulation performed in Extended Data Figure i-l is provided in SI Fig. 3. Code can be found at https://github.com/sfbrunner/chromothripsis-gene-amp-cancer.

References

1. Benner SE, Wahl GM, Von Hoff DD. Double minute chromosomes and homogeneously staining regions in tumors taken directly from patients versus in human tumor cell lines. Anticancer Drugs. 1991; 2:11–25. [PubMed: 1720337]
2. Turner KM, et al. Extrachromosomal oncogene amplification drives tumour evolution and genetic heterogeneity. Nature. 2017; 543:122–125. DOI: 10.1038/nature21356 [PubMed: 28178237]
3. Albertson DG. Gene amplification in cancer. Trends Genet. 2006; 22:447–455. DOI: 10.1016/j.tig.2006.06.007 [PubMed: 16787682]
4. Alt FW, Kellems RE, Bertino JR, Schimke RT. Selective multiplication of dihydrofolate reductase genes in methotrexate-resistant variants of cultured murine cells. J Biol Chem. 1978; 253:1357–1370. [PubMed: 627542]
5. Kaufman RJ, Brown PC, Schimke RT. Amplified dihydrofolate reductase genes in unstably methotrexate-resistant cells are associated with double minute chromosomes. Proc Natl Acad Sci U S A. 1979; 76:5669–5673. [PubMed: 293670]
6. Nunberg JH, Kaufman RJ, Schimke RT, Urlaub G, Chasin LA. Amplified dihydrofolate reductase genes are localized to a homogeneously staining region of a single chromosome in a methotrexate-resistant Chinese hamster ovary cell line. Proc Natl Acad Sci U S A. 1978; 75:5553–5556. [PubMed: 281704]
7. Carroll SM, et al. Double minute chromosomes can be produced from precursors derived from a chromosomal deletion. Mol Cell Biol. 1988; 8:1525–1533. [PubMed: 2898098]
8. Ruiz JC, Wahl GM. Chromosomal destabilization during gene amplification. Mol Cell Biol. 1990; 10:3056–3066. DOI: 10.1128/mcb.10.6.3056 [PubMed: 2188107]
9. Coquelle A, Rozier L, Dutrillaux B, Debatisse M. Induction of multiple double-strand breaks within an hsr by meganucleaseI-SceI expression or fragile site activation leads to formation of double minutes and other chromosomal rearrangements. Oncogene. 2002; 21:7671–7679. DOI: 10.1038/sj.onc.1205880 [PubMed: 12400009]
10. Nathanson DA, et al. Targeted therapy resistance mediated by dynamic regulation of extrachromosomal mutant EGFR DNA. Science. 2014; 343:72–76. DOI: 10.1126/science.1241328 [PubMed: 24310612]
11. Consortium, I. T. P.-C. A. o. W. G. Pan-cancer analysis of whole genomes. Nature. 2020; 578:82–93. DOI: 10.1038/s41586-020-1969-6 [PubMed: 32025007]
12. Li Y, et al. Patterns of somatic structural variation in human cancer genomes. Nature. 2020; 578:112–121. DOI: 10.1038/s41586-019-1913-9 [PubMed: 32025012]
13. Cortes-Ciriano I, et al. Comprehensive analysis of chromothripsis in 2,658 human cancers using whole-genome sequencing. Nat Genet. 2020; doi: 10.1038/s41588-019-0576-7
14. Stephens PJ, et al. Massive genomic rearrangement acquired in a single catastrophic event during cancer development. Cell. 2011; 144:27–40. DOI: 10.1016/j.cell.2010.11.055 [PubMed: 21215367]
15. deCarvalho AC, et al. Discordant inheritance of chromosomal and extrachromosomal DNA elements contributes to dynamic disease evolution in glioblastoma. Nat Genet. 2018; 50:708–717. DOI: 10.1038/s41588-018-0105-0 [PubMed: 29686388]
16. Verhaak RGW, Bafna V, Mischel PS. Extrachromosomal oncogene amplification in tumour pathogenesis and evolution. Nat Rev Cancer. 2019; 19:283–288. DOI: 10.1038/s41568-019-0128-6 [PubMed: 30872802]
17. Rausch T, et al. Genome sequencing of pediatric medulloblastoma links catastrophic DNA rearrangements with TP53 mutations. Cell. 2012; 148:59–71. DOI: 10.1016/j.cell.2011.12.013 [PubMed: 22265402]
18. Nones K, et al. Genomic catastrophes frequently arise in esophageal adenocarcinoma and drive tumorigenesis. Nat Commun. 2014; 5:5224.doi: 10.1038/ncomms6224 [PubMed: 25351503]
19. Ly P, et al. Chromosome segregation errors generate a diverse spectrum of simple and complex genomic rearrangements. Nat Genet. 2019; 51:705–715. DOI: 10.1038/s41588-019-0360-8 [PubMed: 30833795]

20. Singer MJ, Mesner LD, Friedman CL, Trask BJ, Hamlin JL. Amplification of the human dihydrofolate reductase gene via double minutes is initiated by chromosome breaks. Proc Natl Acad Sci U S A. 2000; 97:7921–7926. DOI: 10.1073/pnas.130194897 [PubMed: 10859355]
21. Windle B, Draper BW, Yin YX, O'Gorman S, Wahl GM. A central role for chromosome breakage in gene amplification, deletion formation, and amplicon integration. Genes Dev. 1991; 5:160–174. DOI: 10.1101/gad.5.2.160 [PubMed: 1995414]
22. McClintock B. The Stability of Broken Ends of Chromosomes in Zea Mays. Genetics. 1941; 26:234–282. [PubMed: 17247004]
23. Glodzik D, et al. A somatic-mutational process recurrently duplicates germline susceptibility loci and tissue-specific super-enhancers in breast cancers. Nat Genet. 2017; 49:341–348. DOI: 10.1038/ng.3771 [PubMed: 28112740]
24. Garsed DW, et al. The architecture and evolution of cancer neochromosomes. Cancer Cell. 2014; 26:653–667. DOI: 10.1016/j.ccell.2014.09.010 [PubMed: 25517748]
25. Landry JJ, et al. The genomic and transcriptomic landscape of a HeLa cell line. G3 (Bethesda). 2013; 3:1213–1224. DOI: 10.1534/g3.113.005777 [PubMed: 23550136]
26. Zhang CZ, et al. Chromothripsis from DNA damage in micronuclei. Nature. 2015; 522:179–184. DOI: 10.1038/nature14493 [PubMed: 26017310]
27. Yaeger R, et al. Mechanisms of Acquired Resistance to BRAF V600E Inhibition in Colon Cancers Converge on RAF Dimerization and Are Sensitive to Its Inhibition. Cancer Res. 2017; 77:6513–6523. DOI: 10.1158/0008-5472.CAN-17-0768 [PubMed: 28951457]
28. Ly P, et al. Selective Y centromere inactivation triggers chromosome shattering in micronuclei and repair by non-homologous end joining. Nat Cell Biol. 2017; 19:68–75. DOI: 10.1038/ncb3450 [PubMed: 27918550]
29. Shimizu N, Hashizume T, Shingaki K, Kawamoto JK. Amplification of plasmids containing a mammalian replication initiation region is mediated by controllable conflict between replication and transcription. Cancer Res. 2003; 63:5281–5290. [PubMed: 14500359]
30. Maciejowski J, Li Y, Bosco N, Campbell PJ, de Lange T. Chromothripsis and Kataegis Induced by Telomere Crisis. Cell. 2015; 163:1641–1654. DOI: 10.1016/j.cell.2015.11.054 [PubMed: 26687355]
31. Hoffelder DR, et al. Resolution of anaphase bridges in cancer cells. Chromosoma. 2004; 112:389–397. DOI: 10.1007/s00412-004-0284-6 [PubMed: 15156327]
32. Helleday T, Petermann E, Lundin C, Hodgson B, Sharma RA. DNA repair pathways as targets for cancer therapy. Nat Rev Cancer. 2008; 8:193–204. DOI: 10.1038/nrc2342 [PubMed: 18256616]
33. Cermak T, et al. Efficient design and assembly of custom TALEN and other TAL effector-based constructs for DNA targeting. Nucleic Acids Res. 2011; 39:e82.doi: 10.1093/nar/gkr218 [PubMed: 21493687]
34. Fachinetti D, et al. DNA Sequence-Specific Binding of CENP-B Enhances the Fidelity of Human Centromere Function. Dev Cell. 2015; 33:314–327. DOI: 10.1016/j.devcel.2015.03.020 [PubMed: 25942623]
35. Schindelin J, et al. Fiji: an open-source platform for biological-image analysis. Nat Methods. 2012; 9:676–682. DOI: 10.1038/nmeth.2019 [PubMed: 22743772]
36. Ou HD, et al. ChromEMT: Visualizing 3D chromatin structure and compaction in interphase and mitotic cells. Science. 2017; 357doi: 10.1126/science.aag0025
37. Ou HD, Deerinck TJ, Bushong E, Ellisman MH, O'Shea CC. Visualizing viral protein structures in cells using genetic probes for correlated light and electron microscopy. Methods. 2015; 90:39–48. DOI: 10.1016/j.ymeth.2015.06.002 [PubMed: 26066760]
38. Rao SS, et al. A 3D map of the human genome at kilobase resolution reveals principles of chromatin looping. Cell. 2014; 159:1665–1680. DOI: 10.1016/j.cell.2014.11.021 [PubMed: 25497547]
39. Li H, Durbin R. Fast and accurate long-read alignment with Burrows-Wheeler transform. Bioinformatics. 2010; 26:589–595. DOI: 10.1093/bioinformatics/btp698 [PubMed: 20080505]
40. Raine KM, et al. ascatNgs: Identifying Somatically Acquired Copy-Number Alterations from Whole-Genome Sequencing Data. Curr Protoc Bioinformatics. 2016; 56doi: 10.1002/cpbi.17

41. Nik-Zainal S, et al. Landscape of somatic mutations in 560 breast cancer whole-genome sequences. Nature. 2016; 534:47–54. DOI: 10.1038/nature17676 [PubMed: 27135926]

42. Korbel JO, Campbell PJ. Criteria for inference of chromothripsis in cancer genomes. Cell. 2013; 152:1226–1236. DOI: 10.1016/j.cell.2013.02.023 [PubMed: 23498933]

43. Li Y, et al. Constitutional and somatic rearrangement of chromosome 21 in acute lymphoblastic leukaemia. Nature. 2014; 508:98–102. DOI: 10.1038/nature13115 [PubMed: 24670643]

44. Alexandrov LB, Nik-Zainal S, Wedge DC, Campbell PJ, Stratton MR. Deciphering signatures of mutational processes operative in human cancer. Cell Rep. 2013; 3:246–259. DOI: 10.1016/j.celrep.2012.12.008 [PubMed: 23318258]

Europe PMC Funders Author Manuscripts

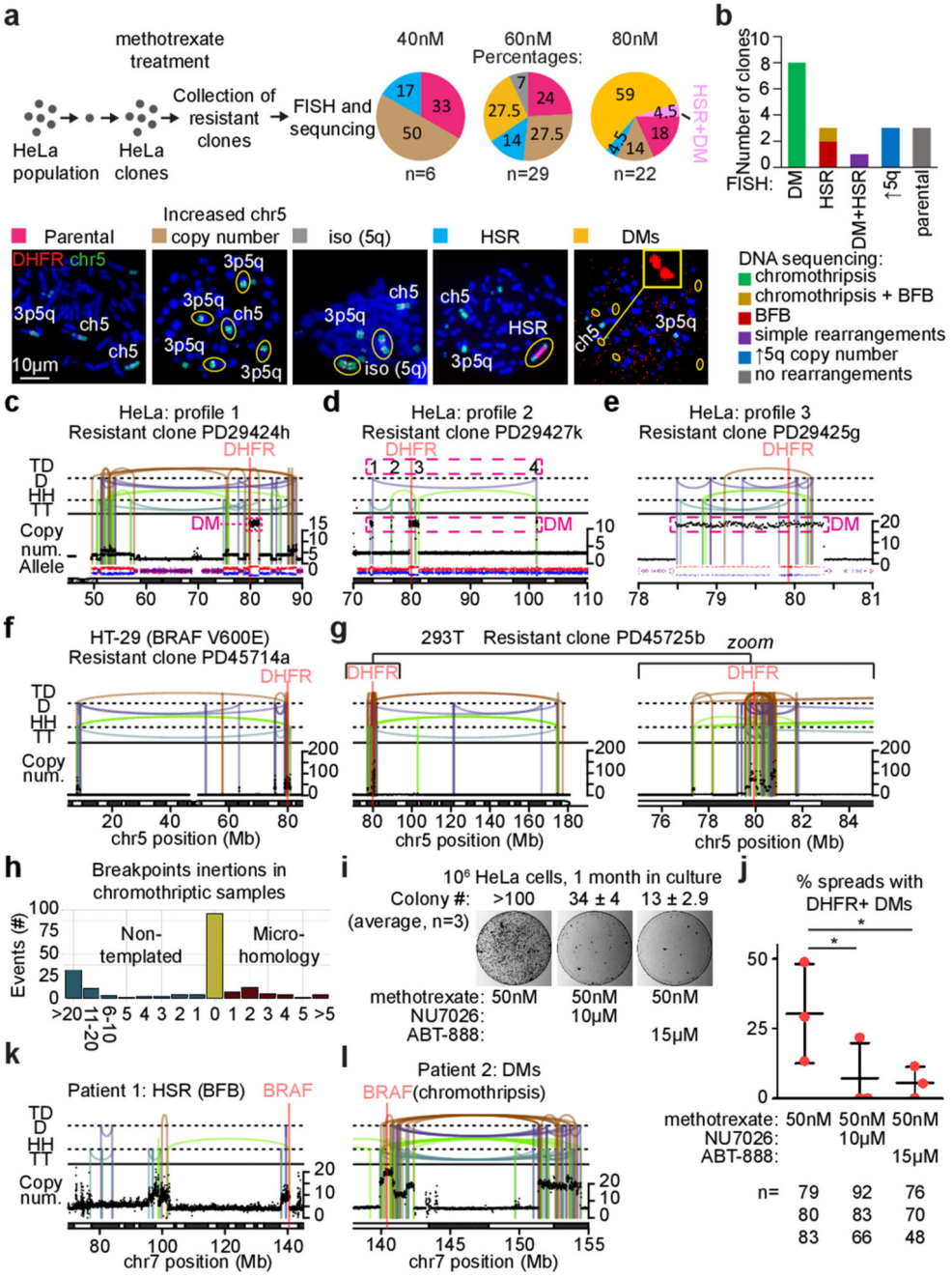

Figure 1. Chromothripsis drives ecDNA formation and amplification as DMs early during drug resistance development in a PARP and NHEJ dependent manner

(**a**) Strategy used to generate unique and independent methotrexate resistant HeLa clones. Pie charts show the distribution of chromosome 5 abnormalities. Representative DNA-FISH images (from the 57 clones) of each abnormality are presented. (**b**) Summary of the genomic mechanisms (determined by whole-genome paired-end sequencing) leading to each type of karyotypic outcome (determined by FISH). (**c-g, k-l**) Copy number and structural variation profiles of (**c-g**) DHFR+ DM+ methotrexate resistant clones and (**k-l**) vemurafenib resistant

Europe PMC Funders Author Manuscripts

patients. Allelic ratios are shown for **c-e**. TD – tandem duplication, D – deletion, HH – head-to-head inversion, TT – tail-to-tail inversion. (**h**) Sequence analysis of structural variation breakpoints in chromothriptic DM HeLa clones. (**i**) Colony assay of methotrexate treated naïve HeLa cells with or without DNA repair inhibition. Images represent three independent experiments. (**j**) Quantification of cells with *DHFR*+ DMs as determined by FISH under indicated conditions. Average of three independent experiments. *p<0.05 (repeated measures one-way ANOVA with post-hoc Tukey test, mean ± s.e.m).

Europe PMC Funders Author Manuscripts

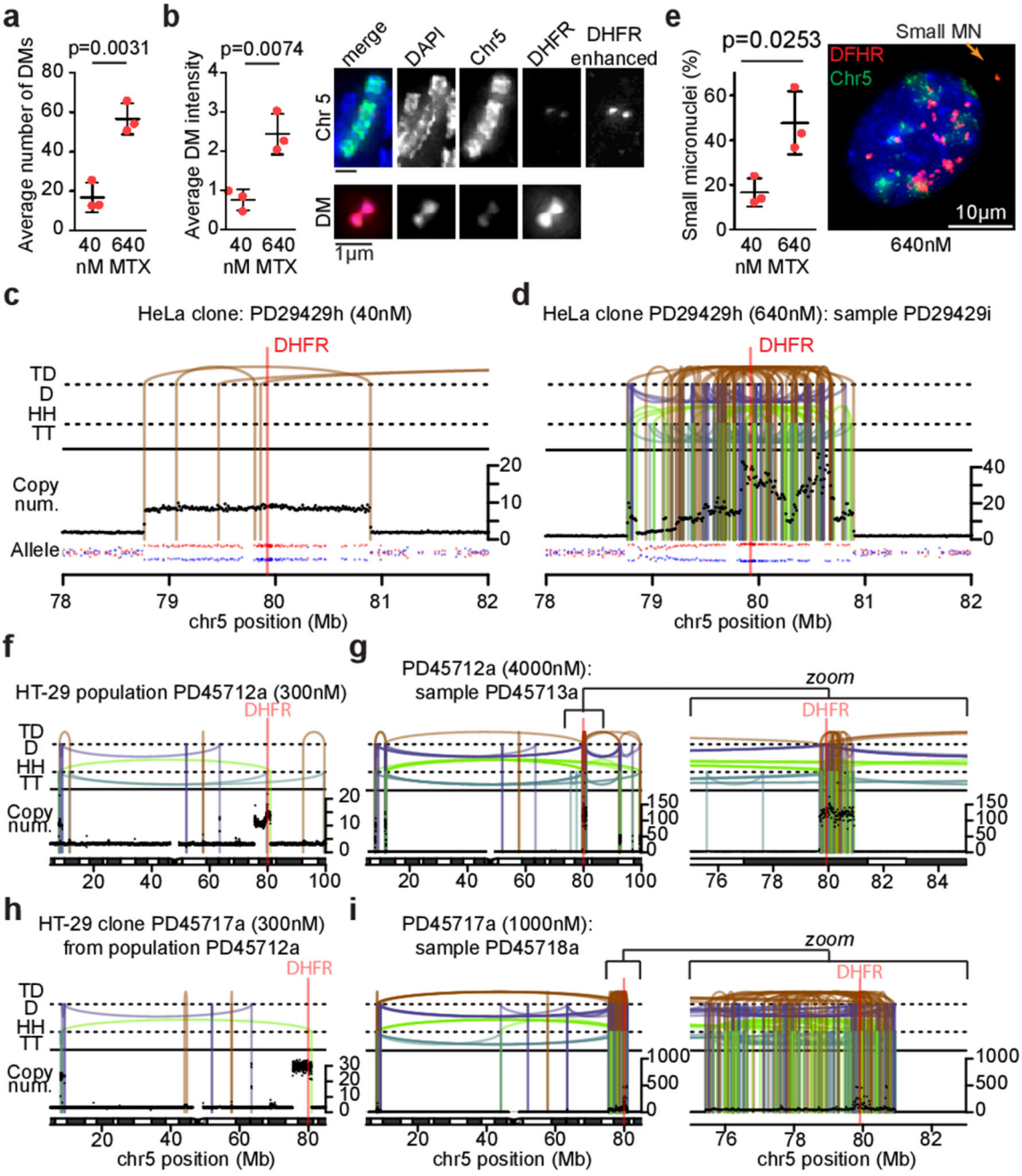

Figure 2. DM structure is optimized by chromothripsis during adaptation to increased selection pressure

(**a**) Quantification of DM numbers using DNA-FISH. Mean ± SD of three independent clones (see Extended Data Fig. 4b) and p-value calculated using two-tailed t-test are presented. (**b**) Left: Average intensity of *DHFR* signal in DMs relative to the intensity of the endogenous *DHFR* signal on chromosome 5 from the same spread, as determined by DNA-FISH. Mean ± SD of three independent DM clones is presented (see Extended Data Fig. 4c). p-value was calculated using two-tailed t-test. Right: DNA-FISH image from a chromosome

Europe PMC Funders Author Manuscripts

Europe PMC Funders Author Manuscripts

spread of clone PD29429i (see Extended Data Fig. 4c) showing a DM with increased signal intensity. (**c-d,f-i**) Copy number and structural variation profiles of indicated samples. Allelic ratios are shown for HeLa clone PD29429h and a derivative population following adaptation to 640nM methotrexate (**c-d)**. A population of HT-29 cells with *DHFR*+ DMs resistant to initial 300nM methotrexate (**f**, PD45712a), and after increasing methotrexate concentration to 4000nM (**g**, PD45713a) are presented. Results of a clone derived from the population (PD45712a) is presented in **h** (PD45717a), also after increasing methotrexate concentration to 1000nM (**i**, sample PD45718a, notice massive rearrangements are different from PD45713a shown in **g**, highlighting the random nature of the rearrangements) are also presented. (**e**) Quantification of *DHFR*+ DM sized (small) micronuclei using DNA-FISH (representative image presented). Mean ± SD of three independent clones and p-value calculated using two-tailed t-test are presented. 40nM: n = 147, 130, 98; 640nM: n = 74, 216, 133.

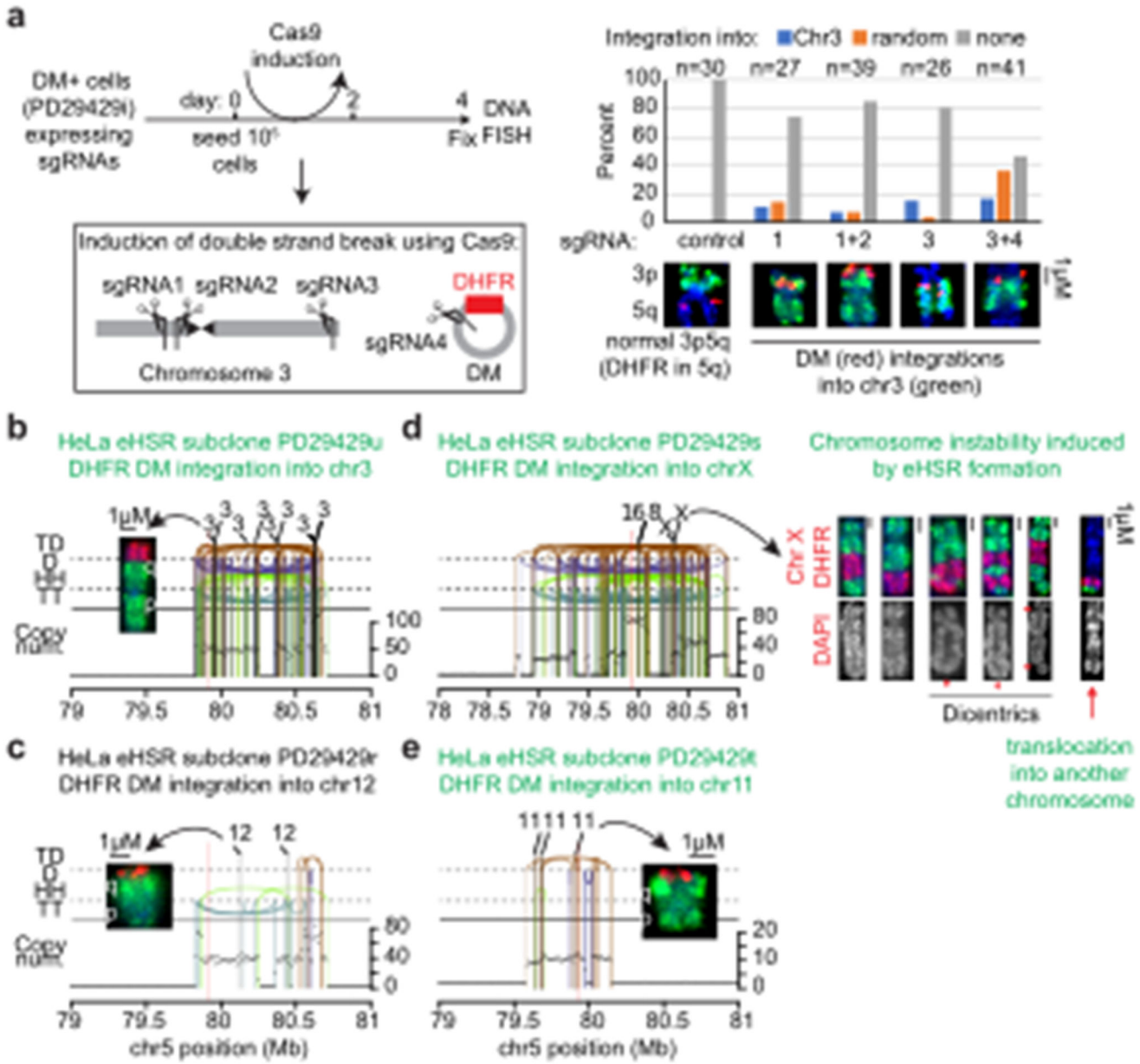

Figure 3. Double minutes preferentially integrate in broken DNA sites near chromosome ends and form ectopic HSRs

(**a**) Quantification of DM integration into ectopic sites on chromosome 3 following double strand break induction using Cas9. DNA-FISH images of chromosomes with DM integration from each experiment are provided (**b-e**) Copy number, structural variation, and translocation profiles of four independent subclones derived from clone PD29429i treated with 1500nM methotrexate and 15μM ABT-888 (PARP inhibitor). DNA-FISH images of chromosomes with DM integration in each clone are provided (integrations observed in all spreads from each clone, n = 15 per clone).

Europe PMC Funders Author Manuscripts

Europe PMC Funders Author Manuscripts

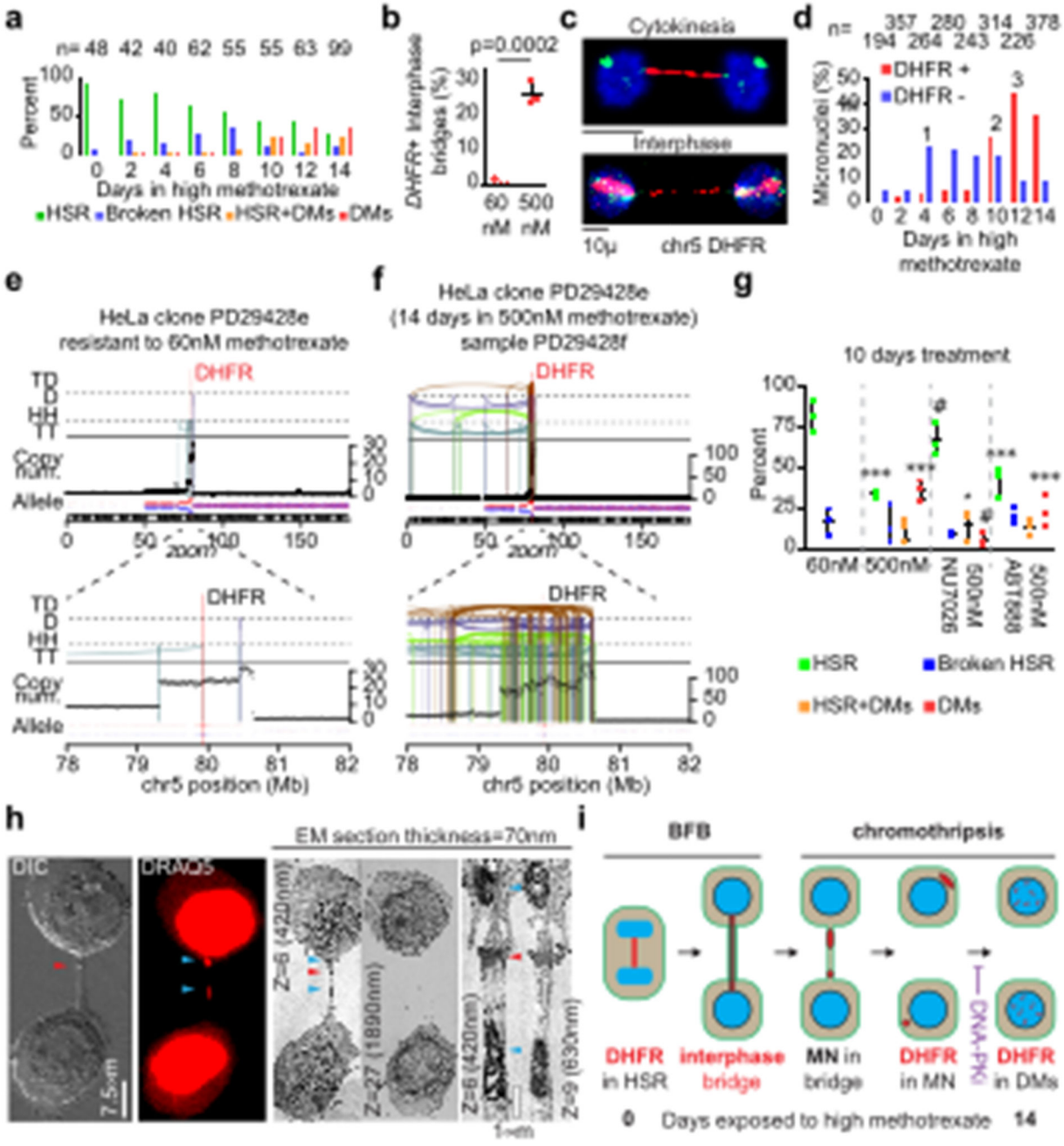

Figure 4. HSRs fragment in interphase bridges and form micronuclei and DMs through chromothripsis and NHEJ repair

(**a**) Location of *DHFR* amplification as determined using DNA-FISH in clone PD29428e over the course of two weeks when exposed to increased methotrexate concentration (500nM) (**b**) Quantification of *DHFR+* interphase bridges in clone PD29428e using DNA-FISH. Mean ± SD of three independent experiments (number of cells scored - 60nM: 144, 221, 204; 12 days in 500nM: 163, 218, 214) and p-value calculated using two-tailed t-test are presented. (**c**) Representative DNA-FISH images of *DHFR*+ interphase bridges (from

data shown in panel b). (**d**) Quantification of *DHFR*+ over the course of two weeks in clone PD29428e exposed to increased methotrexate concentration as determined by DNA-FISH (representative image from the data is shown in Extended Data Fig. 8k). Day 4 (timepoint 1) shows increased *DHFR*-micronuclei (due to the random DNA damage from increased methotrexate). Day 12 (timepoint 2) shows increased *DHFR*+ micronuclei (product of HSR fragmentation), followed by reduction of *DHFR*- micronuclei two days later (timepoint 3). (**e-f**) Copy number and structural variation profiles of indicated samples. (**g**) Quantification of amplification patterns in clone PD29428e exposed to increased methotrexate concentration for 10 days, with or without addition of the DNA repair inhibitors. Bars represent mean ± SD of three independent experiments (spreads counted - 60nM:42, 32, 33; 500nM: 36, 50, 38; 500nM+10μM NU7026: 37, 35, 45; 500nM+15μM ABT-888: 35, 34, 32). *p<0.05, ***p<0.001 (compared to 60nM condition). #p<0.001 (compared to 500nM condition). p-values calculated using two-way ANOVA. (**h**) Correlative light and electron microscopy (CLEM) showing an interphase bridge (of 17 bridges imaged) with micronuclei on both sides (blue arrowheads) of the midbody (red arrowhead). (**i**) Summary of the events underlying BFB-chromothripsis.